

1 **ON NEW STRATEGIES TO CONTROL THE ACCURACY OF WENO
2 ALGORITHMS CLOSE TO DISCONTINUITIES***

3 SERGIO AMAT[†], JUAN RUIZ [‡], AND CHI-WANG SHU [§]

4 **Abstract.** In this paper we construct and analyze new nonlinear optimal weights for WENO
5 interpolation which are capable of raising the order of accuracy close to jump discontinuities in
6 the function or in the first derivative (kinks). The new nonlinear optimal weights are constructed
7 using a strategy inspired by the original WENO algorithm, and they work very well for kinks or jump
8 discontinuities, leading to optimal theoretical accuracy. This is the first part of a series of two papers.
9 In this first part we analyze the performance of the new algorithms proposed for univariate function
10 approximation in the point values (interpolation problem). In the second part, we will extend the
11 analysis to univariate function approximation in the cell averages (reconstruction problem) and to
12 the solution of problems in the context of hyperbolic conservation laws.

13 Our aim is twofold: to raise the order of accuracy of the WENO type interpolation schemes both
14 near discontinuities in the function or in the first derivative (kinks) and in the intervals which contain
15 a kink. The first problem can be solved using the new nonlinear optimal weights, but the second one
16 requires a new strategy that locates the position of the singularity inside the cell in order to attain
17 adaption, this new strategy is inspired by the ENO-SR schemes proposed by Harten in A. Harten,
18 ENO schemes with subcell resolution, J. Comput. Phys. 83 (1) (1989) 148 – 184. Thus, we will
19 introduce two different algorithms in the point values. The first one can deal with kinks and jump
20 discontinuities for intervals not containing the singularity. The second algorithm can also deal with
21 intervals containing kinks, as they can be detected from the point values, but jump discontinuities
22 can not, as the information of their position is lost during the discretization process. As mentioned
23 before, the second part of this work will be devoted to the cell averages and, in this context, it will
24 be possible to work with jump discontinuities as well.

25 **Key words.** WENO schemes, new optimal weights, improved adaption to discontinuities, signal
26 processing.

27 **AMS subject classifications.** 65D05, 65D17, 65M06, 65N06

28 **1. Introduction.** The reconstruction of a piecewise continuous function from
29 some discretized data points is an important problem in the approximation theory.
30 We will consider two possible ways of discretizing the initial set of data: it might
31 come from a sampling of a piecewise continuous function or from the averaging of a
32 function in L^1 over certain intervals. In the first case we are talking about a *point*
33 *value* discretization and in the second case about a *cell average* discretization. This
34 is the first part of a series of two articles where we present a new algorithm for
35 approximation of piecewise smooth functions. In this part we will only consider the
36 point value discretization. The second part [1] will be dedicated to the cell average
37 discretization and its application to the solution of conservation laws.

38 When approximating a function from discretized data, we can choose to use linear
39 or nonlinear algorithms. Linear algorithms usually present accuracy problems when
40 the stencil crosses a discontinuity: Gibbs oscillations usually appear and the accuracy
41 is lost locally around the discontinuity. The increasing of the length of the stencil

*Submitted to the editors September 19th, 2018.

Funding: This work was funded by the *Programa de Apoyo a la investigación de la fundación Séneca-Agencia de Ciencia y Tecnología de la Región de Murcia* 19374/PI/14 and through the national research project MTM2015-64382-P (MINECO/FEDER) and by NSF grant DMS-1719410

[†]Department of Applied Mathematics and Statistics, Universidad Politécnica de Cartagena (UPCT) (Spain), (sergioamat@upct.es),

[‡]Corresponding author. Department of Physics and Mathematics, Universidad de Alcalá (UAH) (Spain), (juan.ruiza@uah.es).

[§]Division of Applied Mathematics, Brown University (USA), (shu@dam.brown.edu).

42 does not solve the problem and usually results in larger zones affected by oscillations.
 43 ENO (essentially non-oscillatory) interpolation solves this problem choosing stencils
 44 that do not cross the discontinuity. This algorithm was introduced in [2, 3] for solving
 45 conservation laws problems. ENO scheme manages to reduce the zones affected by
 46 oscillations to the interval where the discontinuity is placed. This task is done using
 47 a stencil selection strategy which allows us to choose the smoothest stencil. The
 48 reader interested in obtaining more information about ENO algorithm can refer to
 49 the following incomplete list of references [2, 3, 4, 5, 6, 7, 8, 9, 10, 11, 12].

50 In [13], Liu, Osher and Chan proposed WENO (weighted ENO) algorithm, which
 51 aim was to improve the results obtained by ENO method. This technique was pro-
 52 posed in [13] as a nonlinear convex combination of the approximations obtained by
 53 different interpolants constructed over sub-stencils, all of them fragments of a bigger
 54 stencil. The weights used were calculated through an estimation of the smoothness
 55 of the interpolants used.

56 The smoothness of the data is estimated using *smoothness indicators* that are
 57 functions that take divided differences as arguments. In [14] the authors presented
 58 new smoothness indicators which, crucially, were more efficient than those proposed
 59 initially in [13]. The computation of these indicators is done through a measurement
 60 based on the sum of the L^2 norms of the derivatives of the interpolatory polynomials
 61 at the interval where we want to obtain the prediction. The computational cost of
 62 this measurement is smaller than the one obtained using the total variation and its
 63 result is smoother and easier to compute than the total variation. The nonlinear
 64 weights are designed in such a way that the stencils that cross a discontinuity pose an
 65 insignificant contribution to the resulting interpolation. The purpose of the WENO
 66 algorithm proposed in the seminal reference [13] was to optimize the stencil used by
 67 the ENO algorithm at smooth zones, in order to attain a higher order of accuracy.
 68 The interested reader can refer to [5, 15, 16, 17, 18, 19, 20, 21, 22, 23, 24, 25, 26, 27,
 69 28, 29, 30, 31, 32, 33] and especially to [34, 35] and the references therein in order to
 70 get a more complete picture of the state of the art about WENO.

71 As it was originally conceived, the WENO strategy only imposes restrictions to
 72 the weights of the convex combination in smooth zones: the main objective is to
 73 reach maximum order of accuracy when the data is smooth in the whole bigger sten-
 74 cil. However, close to discontinuities the value of the weights is mainly taking care
 75 of the essentially non-oscillatory property, not the order of accuracy, hence the order
 76 of accuracy is not optimized if there is more than one sub-stencil free of discontinu-
 77 ities. Basically, this property of the WENO algorithm is due to the usage of fixed
 78 *optimal-weights* when constructing the nonlinear weights of the convex combination of
 79 interpolants. This problem can be easily appreciated if we perform a grid refinement
 80 analysis around a discontinuity and we obtain the numerical accuracy obtained by
 81 the algorithm. The interested reader can have a look to the experiments presented in
 82 [36], especially Tables 1 and 3 or Figure 5.

83 Our aim in this article is to increase the accuracy of the WENO method close
 84 to kinks or jump discontinuities when the data is discretized in the point values. We
 85 will tackle this task by proposing new nonlinear optimal weights. The main objective
 86 is to attain the maximum theoretical accuracy close to discontinuities in the function
 87 or in the first derivative, while keeping maximum accuracy in smooth zones. New
 88 smoothness indicators were introduced in [36] in order to allow the WENO scheme
 89 to simultaneously detect kinks and jump discontinuities in the point values. At the
 90 same time, these smoothness indicators show the same properties as the original
 91 smoothness indicators proposed in [14]. Using these smoothness indicators we propose

92 two new algorithms. The first one aims to attain optimal control of the accuracy of
 93 the interpolation around discontinuities, but not in the interval that contains the
 94 discontinuity. The objective of the second one is to raise the accuracy of the WENO
 95 algorithm also in the intervals that contain a kink. It is well known that the classical
 96 WENO scheme loses its accuracy when a discontinuity is placed in the central interval
 97 of the stencil. The state of the art literature includes algorithms that try to solve this
 98 issue of the classical WENO scheme. For example, in [37] the authors succeed in
 99 increasing the accuracy of the approximation, but they do not obtain the maximum
 100 accuracy theoretically possible. In this paper we increase the order of accuracy in the
 101 central cell of the stencil and obtain optimal accuracy.

102 This paper is organized as follows: Section 2 introduces the discretization of data
 103 that will be used in the whole article and shows how the WENO algorithm for point
 104 values works. Subsection 2.1 presents a very brief description of the nonlinear WENO
 105 weights. In Subsection 2.2 we review some smoothness indicators that appear in
 106 the literature. Section 3 is devoted to the new WENO algorithm. Subsection 3.1 is
 107 dedicated to the introduction of new smoothness indicators more adapted for working
 108 with kinks. Subsection 3.2 explains how to redesign the WENO optimal weights in
 109 order to control the accuracy close to discontinuities, but not in the interval that
 110 contains the discontinuity. Subsection 3.3 presents a strategy through which we are
 111 able of raising the accuracy in the interval that contains the kink and, at the same time,
 112 controlling the order of accuracy close to it. Subsection 3.4 analyzes the ENO property
 113 for the two algorithms presented. Section 4 is dedicated to test the new algorithms
 114 through some numerical experiments. In particular, we analyze the performance of
 115 the new algorithm using discretized univariate functions that show kinks and jump
 116 discontinuities. Finally, Section 5 presents the conclusions.

117 **2. Weighted essentially non-oscillatory (WENO) algorithm for point
 118 values.** In this section we introduce the classical WENO method. The concepts
 119 presented in this section are already classic and can be found in many references, see
 120 for example [13, 14, 36, 37], but their presence is strictly necessary to keep the paper
 121 self-contained and to introduce the different notations that we will use.

122 Let us consider the space of finite sequences V , a uniform partition X of the
 123 interval $[a, b]$ in J subintervals, and the set of piecewise continuous functions in the
 124 interval $[a, b]$,

$$X = \{x_i\}_{i=0}^J, \quad x_0 = a, \quad h = x_i - x_{i-1}, \quad x_J = b.$$

125 We will use a point value discretization of the data,

$$f_i = f(x_i), \quad f = \{f_i\}_{i=0}^J.$$

126 We can see that the previous discretization preserves the information locally at the
 127 sites x_i . Although it is possible to locate the position of kinks, as shown in Figure
 128 1, there is no hope in locating the exact positions of jumps, as they are lost in
 129 the discretization process [38], as shown in Figure 2. We will always consider that
 130 discontinuities are far enough from each other (for WENO algorithm and stencils of
 131 6 points we will consider that we have at least four discretization grid-points between
 132 any adjacent discontinuities).

133 In this section we introduce the WENO scheme. As mentioned before, this algo-
 134 rithm allows us to obtain a high order of accuracy at smooth zones of f and, at the
 135 same time, it manages to avoid Gibbs oscillations close to discontinuities. This tech-
 136 nique appeared as an improvement of ENO reconstructions [2, 3]. The ENO scheme

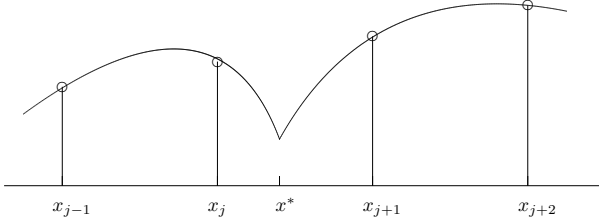


FIG. 1. This figure represents a kink placed in the interval (x_j, x_{j+1}) at a position x^* . If we consider that the discretized data is in the point values, we can recover an approximation of the position of the discontinuity crossing an interpolating polynomial built using the data to the right of the discontinuity with another interpolating polynomial built using the data to the left.

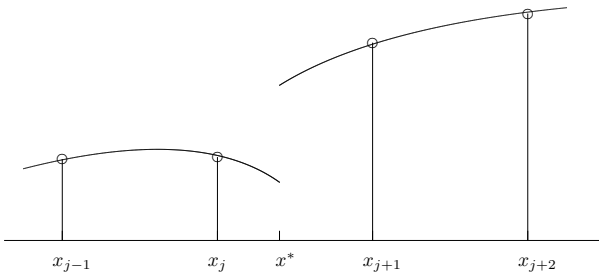


FIG. 2. This figure represents a jump discontinuity placed in the interval (x_j, x_{j+1}) at a position x^* . In this case it is not possible to recover the position of the discontinuity from the discretized data in the point values [38].

133 uses a stencil selection procedure and manages to obtain an order of accuracy $r + 1$.
 134 In order to do this, this scheme deals with several stencils of length $r + 1$. The ENO
 135 scheme uses divided differences in order to determine which stencil is the smoothest.
 136 The WENO scheme uses smoothness indicators based on (divided) differences to de-
 137 termine the smoothness of the stencil.

138 We will denote the different stencils by $S_i^m(j) = \{x_{j-m+i}, \dots, x_{j+i-1}\}$. The
 139 WENO scheme uses the same stencil of $2r$ nodes $S_r^{2r}(j) = \{x_{j-r}, \dots, x_{j+r-1}\}$ as the
 140 ENO method when trying to interpolate in the interval (x_{j-1}, x_j) . Using this stencil,
 141 WENO manages to reach order of accuracy $2r$ [13] at smooth regions of f . In our
 142 notation, $S_k^r(j)$, $k = 0, \dots, r - 1$ will represent the r sub-stencils of length $r + 1$ that
 143 contains the interval (x_{j-1}, x_j) , where we want to interpolate:

144 (2.1)
$$S_k^r(j) = \{x_{j-r+k}, \dots, x_{j+k}\}, \quad k = 0, \dots, r - 1.$$

145 Figure 3 presents a diagram where we show the big stencil $S_r^{2r}(j)$ and the sub-stencils
 146 $S_k^r(j)$, $k = 0, \dots, r - 1$ considered for the particular case $r = 3$.

147 Let's consider the following convex combination,

148 (2.2)
$$q_{j-r}(x) = \sum_{k=0}^{r-1} \omega_k^r(j) p_{j-r+k}^r(x),$$

149 where $\omega_k^r(j) \geq 0$, $k = 0, \dots, r - 1$ and $\sum_{k=0}^{r-1} \omega_k^r(j) = 1$. In (2.2), $p_{j-r+k}^r(x)$ represents
 150 the interpolatory polynomial of degree r defined on the stencil $S_k^r(j)$. The prediction

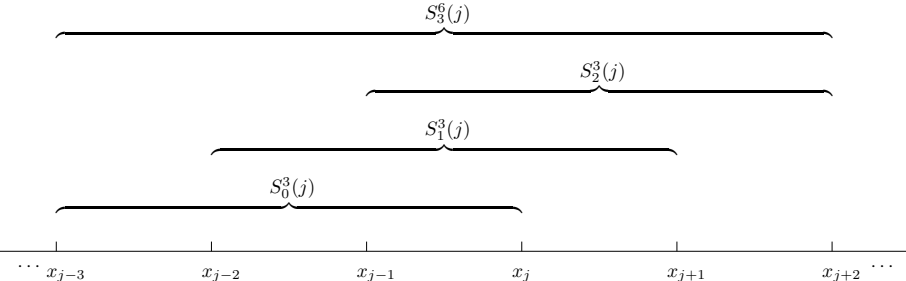


FIG. 3. In this diagram we represent for $r = 3$ the big stencil $S_r^{2r}(j) = \{x_{j-r}, \dots, x_{j+r-1}\}$ and the substencils $S_k^r(j) = \{x_{j-r+k}, \dots, x_{j+k}\}$ for $k = 0, \dots, r-1$.

151 operator for the mid point of the target interval (x_{j-1}, x_j) is given by

152 (2.3)
$$I\left(x_{j-\frac{1}{2}}; f\right) = \sum_{k=0}^{r-1} \omega_k^r(j) p_{j-r+k}^r\left(x_{j-\frac{1}{2}}\right).$$

153 The value of the weights is chosen in order to obtain order of accuracy $2r$ at $x_{j-\frac{1}{2}}$ at
154 smooth regions of the function f . In [13], the authors use an interpolant satisfying,

155 (2.4)
$$p_{j-r}^{2r-1}\left(x_{j-\frac{1}{2}}\right) = f\left(x_{j-\frac{1}{2}}\right) + O(h^{2r}),$$

156 on the big stencil $\{x_{j-r}, \dots, x_{j+r-1}\}$, if we suppose that the function is smooth there.
157 We can also build r approximations

158 (2.5)
$$p_{j-r+k}^r\left(x_{j-\frac{1}{2}}\right) = f\left(x_{j-\frac{1}{2}}\right) + O(h^{r+1}),$$

159 using the small stencils $S_k^r(j)$. The optimal linear weights must satisfy that $C_k^r(j) \geq$
160 $0, \forall k$ and also that $\sum_{k=0}^{r-1} C_k^r(j) = 1$, such that

161 (2.6)
$$p_{j-r}^{2r-1}\left(x_{j-\frac{1}{2}}\right) = \sum_{k=0}^{r-1} C_k^r(j) p_{j-r+k}^r\left(x_{j-\frac{1}{2}}\right).$$

162 The formulae for the optimal weights are easy to obtain if we use Newton interpolating
163 polynomials. In [16], the authors give a proof for the following expression,

164 (2.7)
$$C_k^r(j) = \frac{1}{2^{2r-1}} \binom{2r}{2k+1}, \quad k = 0, \dots, r-1.$$

165 For $r = 3$ the optimal weights are $C_0^3(j) = \frac{3}{16}, C_1^3(j) = \frac{10}{16}, C_2^3(j) = \frac{3}{16}$. In fact, in [39]
166 the authors prove that the weights $C_k^r(j)$ can be written as polynomials. However,
167 we are usually interested in computing the reconstruction in specific points of the
168 considered interval. In this case the polynomials $C_k^r(j)$ take some specific positive
169 values. We will consider this case.

170 **2.1. Nonlinear weights.** In [13], the non linear weights $\omega_k^r(j)$ are designed to
 171 satisfy the following relation at smooth zones,

172 (2.8)
$$\omega_k^r(j) = C_k^r(j) + O(h^m), \quad k = 0, \dots, r-1$$

173 with $m \leq r-1$. Then, at these zones the interpolation error satisfies,

174 (2.9)
$$f(x_{j-\frac{1}{2}}) - q_{j-r}(x_{j-\frac{1}{2}}) = O(h^{r+m+1}).$$

175 When $m = r-1$ in (2.8), (2.9) assures that the accuracy attained is $2r$. That said
 176 accuracy is the same as the one obtained using the interpolant $p_{j-r}^{2r-1}(x)$ that uses
 177 all the nodes in the big stencil. The weights must also be designed in such a way
 178 that they satisfy the ENO property. This means that the contribution to the convex
 179 combination (2.3) of polynomials built from stencils crossing discontinuities should be
 180 insignificant. As mentioned in [13], the weights should also be easy to compute. The
 181 expression for the weights is,

182 (2.10)
$$\omega_k^r(j) = \frac{\alpha_k^r(j)}{\sum_{i=0}^{r-1} \alpha_i^r(j)}, \quad = 0, \dots, r-1 \text{ where } \alpha_k^r(j) = \frac{C_k^r(j)}{(\epsilon + I_k^r(j))^t}.$$

183 This expression for the weights satisfies that $\sum_k \omega_k^r(j) = 1$. In (2.10) $I_k^r(j)$ represents
 184 a smoothness indicator for $f(x)$ on the stencil $S_k^r(j)$. t is an integer that has the
 185 purpose of assuring the maximum order of accuracy close to the discontinuities. The
 186 value of this parameter varies in the literature. For example, in [14] the authors choose
 187 $t = 2$ and in [13], it is set to $t = r$. In the theoretical proofs about the accuracy, we will
 188 determine which value of t we should take in our algorithm. The positive parameter
 189 ϵ that appears in the denominator of (2.10) is included to avoid divisions by zero.
 190 Some references can be found in the literature [15, 16], where the authors prove that
 191 ϵ plays a role when we are interpolating close to critical points at smooth zones. In
 192 this article we will show that the smoothness indicators used satisfy the requirements
 193 exposed in [13, 16] and necessary to attain the desired accuracy. We will also analyze
 194 the role played by the parameter ϵ and explicitly set the value it must take in order
 195 to obtain optimal results with the new algorithms presented.

196 As we will refer all the time to the big stencil $S_r^{2r}(j)$ and in order to ease the
 197 notation, we will drop (j) in $S_k^r(j), \omega_k^r(j), C_k^r(j), \alpha_k^r(j)$ and use simply $S_k^r, \omega_k^r, C_k^r, \alpha_k^r$.

198 **2.2. Classical smoothness indicators.** As mentioned before, the computation
 199 of the smoothness indicators is done through a measurement based on the sum of the
 200 L^2 norms of the derivatives of the interpolatory polynomials at the interval where we
 201 want to obtain the prediction [14],

202 (2.11)
$$I_k^r(j) = \sum_{l=1}^{r-1} h^{2l-1} \int_{x_{j-\frac{1}{2}}}^{x_{j+\frac{1}{2}}} \left(\frac{d^l}{dx^l} p_{j-r+k}^r(x) \right)^2 dx.$$

203 In [16] another expression for the smoothness indicators is introduced, this time for
 204 data discretized in the point values,

205 (2.12)
$$I_k^r(j) = \sum_{l=1}^r h^{2l-1} \int_{x_{j-1}}^{x_j} \left(\frac{d^l}{dx^l} p_{j-r+k}^r(x) \right)^2 dx.$$

206 The smoothness indicators presented before are suitable for jump discontinuities, but
 207 they do not work well for kinks.

208 In [36] we propose a new expression for the smoothness indicators that works well
 209 for kinks and for data discretized in the point values,

210 (2.13)
$$I_k^r(j) = \sum_{l=2}^r h^{2l-1} \int_{x_{j-\frac{1}{2}}}^{x_{j+\frac{1}{2}}} \left(\frac{d^l}{dx^l} p_{j-r+k}^r(x) \right)^2 dx.$$

211 This is the smoothness indicator used for computation of Hamilton-Jacobi equations
 212 [40], for which kinks are the generic singularities in the viscosity solutions.

213 **3. The new WENO algorithm for point values.** In this section we intro-
 214 duce the new WENO algorithm. The difference with the classical WENO algorithm
 215 introduced in previous section is mainly located in the design of the WENO weights.
 216 We also make use of new smoothness indicators more suitable for working in the point
 217 values.

218 **3.1. New smoothness indicators.** The smoothness indicator in (2.13) inte-
 219 grates in the interval $(x_{j-\frac{1}{2}}, x_{j+\frac{1}{2}})$, but it seems more logical to integrate in the
 220 interval (x_{j-1}, x_j) , where the point where we will interpolate is in the middle. Thus,
 221 in this article we propose to use the smoothness indicators in the point values given
 222 by the expression

223 (3.1)
$$I_k^n(j) = \sum_{l=2}^{\min(r,n)} h^{2l-1} \int_{x_{j-1}}^{x_j} \left(\frac{d^l}{dx^l} p_{j-r+k}^n(x) \right)^2 dx,$$

224 where n is the degree of the polynomial and goes from $n = r-1, \dots, 2r-1$. As we will
 225 see in Subsection 3.2, for $r = 3$ our algorithms make use of smoothness indicators of 3,
 226 4, 5 and 6 points in order to optimize the accuracy of the new nonlinear interpolation
 227 proposed. Thus, we will need to build polynomials from degree two to five with the
 228 aim of replacing in (3.1) and obtaining such smoothness indicators. We work with
 229 the stencil of six points $S_3^6 = \{x_{j-3}, x_{j-2}, x_{j-1}, x_j, x_{j+1}, x_{j+2}\}$ and we will obtain the
 230 smoothness indicators integrating in the interval (x_{j-1}, x_j) . The point values used
 231 will be $\{f_{j-3}, f_{j-2}, f_{j-1}, f_j, f_{j+1}, f_{j+2}\}$.

232 In order to obtain compact expressions for the smoothness indicators in terms
 233 of finite differences, the polynomials can be expressed in the Newton form. The
 234 polynomials of degree n starting at the node j have the form,

(3.2)
$$p_j^n(x) = f_j + \frac{f_{j+1} - f_j}{h} (x - x_j) + \frac{f_j - 2f_{j+1} + f_{j+2}}{2h^2} (x - x_j)(x - x_{j+1})$$

$$+ \frac{-f_j + 3f_{j+1} - 3f_{j+2} + f_{j+3}}{6h^3} (x - x_j)(x - x_{j+1})(x - x_{j+2}) + \dots + \frac{\delta_j^n}{n!h^n} \prod_{k=j}^{j+n-1} (x - x_k),$$

235 where $\delta_j^n = f[x_j, \dots, x_{j+n}]h^n$ are finite differences of order n . Using a stencil of six
 236 points, we can build four different polynomials of degree two $\{p_{j-3}^2(x), p_{j-2}^2(x),$
 237 $p_{j-1}^2(x), p_j^2(x)\}$, three of degree three $\{p_{j-3}^3(x), p_{j-2}^3(x), p_{j-1}^3(x)\}$, two of degree four
 238 $\{p_{j-3}^4(x), p_{j-2}^4(x)\}$ and one of degree five $\{p_{j-1}^5(x)\}$. We have used the notation
 239 p_{j-r+k}^n , for $r = 3$. We will use all of these polynomials to obtain smoothness indicators.
 240 As before, we will drop (j) in the notation of the smoothness indicators $I_k^r(j)$ and
 241 simply use I_k^r .

242 The smoothness indicators of three points obtained through (3.1) for $n = r-1 = 2$
 243 and the polynomials $\{p_{j-3}^2(x), p_{j-2}^2(x), p_{j-1}^2(x), p_j^2(x)\}$ can be expressed in terms of

245 finite differences as,

$$\begin{aligned}
 246 \quad (3.3) \quad I_{-1}^2 &= (\delta_{j-3}^2)^2, \\
 I_0^2 &= (\delta_{j-2}^2)^2, \\
 I_1^2 &= (\delta_{j-1}^2)^2, \\
 I_2^2 &= (\delta_j^2)^2,
 \end{aligned}$$

247 with $\delta_i^2 = f_i - 2f_{i+1} + f_{i+2}$. The smoothness indicators of four points obtained
 248 through (3.1) for $n = r = 3$ and the polynomials in $\{p_{j-3}^3(x), p_{j-2}^3(x), p_{j-1}^3(x),\}$ can
 249 be expressed in terms of finite differences as,

$$\begin{aligned}
 250 \quad (3.4) \quad I_0^3 &= \frac{10}{3}(\delta_{j-3}^3)^2 + 3\delta_{j-3}^3\delta_{j-3}^2 + (\delta_{j-3}^2)^2, \\
 I_1^3 &= \frac{4}{3}(\delta_{j-2}^3)^2 + \delta_{j-2}^3\delta_{j-2}^2 + (\delta_{j-2}^2)^2, \\
 I_2^3 &= \frac{4}{3}(\delta_{j-1}^3)^2 - \delta_{j-1}^3\delta_{j-1}^2 + (\delta_{j-1}^2)^2,
 \end{aligned}$$

251 with $\delta_i^3 = -f_i + 3f_{i+1} - 3f_{i+2} + f_{i+3}$. The smoothness indicators of five points
 252 obtained using the same process and the polynomials $\{p_{j-3}^4(x), p_{j-2}^4(x)\}$ are,
 253 (3.5)

$$\begin{aligned}
 I_0^4 &= \frac{19}{6}\delta_{j-3}^4\delta_{j-3}^3 + \frac{2}{3}\delta_{j-3}^4\delta_{j-3}^2 + \frac{547}{240}(\delta_{j-3}^4)^2 + \frac{10}{3}(\delta_{j-3}^3)^2 + 3\delta_{j-3}^3\delta_{j-3}^2 + (\delta_{j-3}^2)^2 \\
 I_1^4 &= \frac{89}{80}(\delta_{j-2}^4)^2 - \frac{1}{6}\delta_{j-2}^4\delta_{j-2}^3 - \frac{1}{3}\delta_{j-2}^4\delta_{j-2}^2 + \frac{4}{3}(\delta_{j-2}^3)^2 + \delta_{j-2}^3\delta_{j-2}^2 + (\delta_{j-2}^2)^2,
 \end{aligned}$$

254 with $\delta_i^4 = f_i - 4f_{i+1} + 6f_{i+2} - 4f_{i+3} + f_{i+4}$. The smoothness indicator of six points
 255 obtained using the same process and the polynomial $p_{j-3}^5(x)$ is,

$$\begin{aligned}
 256 \quad (3.6) \quad I_0^5 &= \frac{1727}{1260}(\delta_{j-3}^5)^2 + \frac{203}{240}\delta_{j-3}^5\delta_{j-3}^4 - \frac{13}{30}\delta_{j-3}^5\delta_{j-3}^3 - \frac{1}{6}\delta_{j-3}^5\delta_{j-3}^2 \\
 &+ \frac{19}{6}\delta_{j-3}^3\delta_{j-3}^4 + \frac{2}{3}\delta_{j-3}^2\delta_{j-3}^4 + \frac{547}{240}(\delta_{j-3}^4)^2 + \frac{10}{3}(\delta_{j-3}^3)^2 + 3\delta_{j-3}^2\delta_{j-3}^3 + (\delta_{j-3}^2)^2,
 \end{aligned}$$

257 with $\delta_i^5 = -f_i + 5f_{i+1} - 10f_{i+2} + 10f_{i+3} - 5f_{i+4} + f_{i+5}$. To obtain these expressions
 258 we have applied the formula in (3.1) integrating always in the interval (x_{j-1}, x_j) .

THEOREM 3.1. At smooth zones, the smoothness indicators (3.4), (3.5) and (3.6) calculated using the expression in (3.1) can be simplified to

$$I_k^n = \left(h^2 f''_{j-1/2} \right)^2 \cdot (1 + O(h^2)), \quad n = 3, 4, 5.$$

259 *Proof.* At smooth zones, obtaining the Taylor expansion of the values of the stencil
 260 $\{f_{j-3}, f_{j-2}, f_{j-1}, f_j, f_{j+1}, f_{j+2}\}$ around $x_{j-1/2}$ and replacing them in the expressions
 261 of the smoothness indicators in (3.4), (3.5) and (3.6), we obtain that I_0^4, I_1^4 and I_0^5 are

262 equal to D_1 , I_0^3 and I_2^3 are equal to D_2 and I_1^3 is equal to D_3 , with

$$\begin{aligned}
 D_1 &= h^4 \left(\frac{d^2 f}{dx^2} (x_{j-1/2}) \right)^2 + \frac{13}{12} h^6 \left(\frac{d^3 f}{dx^3} (x_{j-1/2}) \right)^2 \\
 &\quad + \frac{1}{12} h^6 \left(\frac{d^2 f}{dx^2} (x_{j-1/2}) \right) \frac{d^4 f}{dx^4} (x_{j-1/2}) + O(h^7). \\
 D_2 &= h^4 \left(\frac{d^2 f}{dx^2} (x_{j-1/2}) \right)^2 + \frac{13}{12} h^6 \left(\frac{d^3 f}{dx^3} (x_{j-1/2}) \right)^2 \\
 &\quad - \frac{7}{12} h^6 \left(\frac{d^2 f}{dx^2} (x_{j-1/2}) \right) \frac{d^4 f}{dx^4} (x_{j-1/2}) + O(h^7). \\
 D_3 &= h^4 \left(\frac{d^2 f}{dx^2} (x_{j-1/2}) \right)^2 + \frac{13}{12} h^6 \left(\frac{d^3 f}{dx^3} (x_{j-1/2}) \right)^2 \\
 &\quad + \frac{5}{12} h^6 \left(\frac{d^2 f}{dx^2} (x_{j-1/2}) \right) \frac{d^4 f}{dx^4} (x_{j-1/2}) + O(h^7).
 \end{aligned} \tag{3.7}$$

264 Collecting $h^4 \left(\frac{d^2 f}{dx^2} (x_{j-1/2}) \right)^2$, we get the result. \square

3.2. Obtaining optimal weights close to discontinuities in the point

265 **values.** If the optimal weights are obtained close to a discontinuity in the way specified in (2.6) without any other consideration, the accuracy can be lost when there 266 is more than one smooth substencil. A representation of a typical example of this 267 situation is shown in Figures 4 and 5. The idea is that when a stencil is affected by 268 a discontinuity, WENO is not designed to use all the available smooth information. 269 In fact, the only conditions imposed to obtain the weights of the convex combination 270 of polynomials of WENO interpolation in (2.2) is that they must depend on the 271 smoothness of the function (they are large if the corresponding sub-stencil is smooth 272 and small otherwise), and that at smooth zones the convex combination must provide 273 optimal accuracy. For example, if we are working with stencils of 6 points and a 274 convex combination of three polynomials of degree 3, then, in a situation like the 275 ones depicted in Figures 4 and 5, WENO interpolation will typically provide $O(h)$ 276 accuracy at the interval that contains the discontinuity and $O(h^4)$ accuracy at the 277 other intervals of the stencils that are affected by the discontinuity, even though 278 there is available information to obtain $O(h^5)$ accuracy at the point $x_{j-1/2}$ shown in 279 Figures 4 and 5. If we obtain $O(h^5)$ accuracy in the mentioned interval, it is just by 280 coincidence, as the weights as originally proposed in [14] are not designed to optimize 281 the use of the stencil. It is possible to optimize the weights of the convex combination 282 making the optimal weights also depend on the smoothness of the function, such that 283 the optimal order is attained in all the stencils affected by the discontinuity. 284

285 In this case, we will analyze how to attain optimal order with exactly the same 286 stencil and sub-stencils that WENO method uses. Thus, we will use the formula 287 for the interpolant in (2.3). In order to ease the presentation of the new 288 optimal weights, we analyze the case $r = 3$ that corresponds to $n = 2r = 6$ points. 289 Let's start with the three stencils of four points $S_0^3 = \{x_{j-3}, x_{j-2}, x_{j-1}, x_j\}$, $S_1^3 =$ 290 $\{x_{j-2}, x_{j-1}, x_j, x_{j+1}\}$ and $S_2^3 = \{x_{j-1}, x_j, x_{j+1}, x_{j+2}\}$. The point values used will be 291 $\{f_{j-3}, f_{j-2}, f_{j-1}, f_j, f_{j+1}, f_{j+2}\}$. With these conditions, it is straightforward to build 292 polynomials in the Newton form shown in (3.2). We can denote them by $p_{j-3+k}^3(x)$, 293 such that $r = 3$ denotes the degree of the polynomial and $j - 3 + k$ the node where 294 the substencil starts. Nevertheless, it is more convenient to ease again the notation 295

296 dropping the dependence with j and simply write $p_k^r(x)$, as we will be referring all
 297 the time to the stencil $S_3^6 = \{x_{j-3}, x_{j-2}, x_{j-1}, x_j, x_{j+1}, x_{j+2}\}$. All the polynomials
 298 are evaluated at the point of interpolation $x_{j-1/2}$, as shown in Figures 4 and 5. Then
 299 for $r = 3$ we will be dealing with $p_0^3(x), p_1^3(x)$ and $p_2^3(x)$ for the convex combination
 300 in (2.6) and $p_0^4(x), p_1^4(x), p_2^5(x)$ for calculating the nonlinear optimal weights. It is
 301 straightforward to prove that taking the weights shown in (2.7) for $r = 3$,

$$302 \quad (3.8) \quad \begin{aligned} p_0^4(x) &= 2C_0^3 p_0^3(x) + C_1^3 p_1^3(x) \\ p_1^4(x) &= C_1^3 p_1^3(x) + 2C_2^3 p_2^3(x), \end{aligned}$$

303 with C_0^3, C_1^3 , and C_2^3 the optimal weights for $r = 3$ presented in (2.7). It is clear
 304 that in the case represented in Figure 5 it would be convenient to use $p_1^4(x)$ in order
 305 to interpolate at $x_{j-1/2}$ (and for the case presented in Figure 4, $p_0^4(x)$ is the best
 306 option). However, the WENO scheme does not assure that the convex combination of
 307 $p_0^3(x_{j-1/2})$ and $p_1^3(x_{j-1/2})$ will be equal to $p_0^4(x_{j-1/2})$. If the discontinuity is located
 308 in the intervals (x_{j-2}, x_{j-1}) or (x_j, x_{j+1}) , WENO should obtain $O(h^4)$ accuracy as
 309 there is always a smooth stencil of four points. In order to assure maximum accuracy,
 310 we can design three vectors of optimal weights $\mathbf{C}_0^4, \mathbf{C}_0^5, \mathbf{C}_1^4$, each of which is suitable
 311 for a particular position of the discontinuity. The vectors will have the following
 312 expression,

$$313 \quad (3.9) \quad \mathbf{C}_0^4 = (2C_0^3, C_1^3, 0),$$

$$314 \quad (3.10) \quad \mathbf{C}_0^5 = (C_0^3, C_1^3, C_2^3),$$

$$315 \quad (3.11) \quad \mathbf{C}_1^4 = (0, C_1^3, 2C_2^3).$$

316 \mathbf{C}_0^4 is appropriate in the case presented in Figure 4. \mathbf{C}_1^4 is adequate for the case
 317 in Figure 5. Finally, \mathbf{C}_0^5 works well when there is no discontinuity. A weighted
 318 average of these vectors will result in non-linear optimal weights that would replace
 319 the optimal weights of WENO algorithm. The weights of the mentioned average
 320 will be computed using the same technique introduced in [14] for averaging WENO
 321 interpolatory polynomials: smoothness indicators. Thus, in order to assure optimal
 322 accuracy, we will use smoothness indicators for the polynomials of 4, 5 and 6 points
 323 that arise from the selected 6 points stencil. Let's now denote by $\tilde{\omega}_k^n$ the quotients,

$$324 \quad (3.12) \quad \tilde{\omega}_0^4 = \frac{\tilde{\alpha}_0^4}{\tilde{\alpha}_0^4 + \tilde{\alpha}_0^5 + \tilde{\alpha}_1^4}, \quad \tilde{\omega}_0^5 = \frac{\tilde{\alpha}_0^5}{\tilde{\alpha}_0^4 + \tilde{\alpha}_0^5 + \tilde{\alpha}_1^4}, \quad \tilde{\omega}_1^4 = \frac{\tilde{\alpha}_1^4}{\tilde{\alpha}_0^4 + \tilde{\alpha}_0^5 + \tilde{\alpha}_1^4},$$

325 with,

$$326 \quad (3.13) \quad \tilde{\alpha}_0^4 = \frac{1}{(\epsilon + I_0^4)^t}, \quad \tilde{\alpha}_0^5 = \frac{1}{(\epsilon + I_0^5)^t}, \quad \tilde{\alpha}_1^4 = \frac{1}{(\epsilon + I_1^4)^t}.$$

327 Now we can just define the adapted optimal weights as,

$$328 \quad (3.14) \quad (\tilde{C}_0^3, \tilde{C}_1^3, \tilde{C}_2^3) = \tilde{\omega}_0^4 \mathbf{C}_0^4 + \tilde{\omega}_0^5 \mathbf{C}_0^5 + \tilde{\omega}_1^4 \mathbf{C}_1^4.$$

329 These nonlinear optimal weights \tilde{C}_k^r are used in place of the optimal weights C_k^r in
 330 the expression (2.10). The smoothness indicators that appear in (2.10) are obtained
 331 using four points, and have the expression shown in (3.4). We keep this part of the
 332 algorithm untouched and we only modify the optimal weights, that now are nonlinear.

333 A first explanation of why this technique works is the following:

334 • If all the sub-stencils S_k^n , $n = 3, 4, 5$, (three of four points, two of five points
 335 and one of six points) are smooth and $f''_{j-1/2} \neq 0$, all of them are $I_k^n =$
 336 $(h^2 f''_{j-1/2})^2 \cdot (1 + O(h^2))$, $n = 3, 4, 5$ (as shown in Theorem 3.1). Then, at su-
 337 fficiently smooth zones, the nonlinear weights in (3.12) satisfy the expression

$$(3.15) \quad \tilde{\omega}_k^n = \frac{\tilde{\alpha}_k^n}{\sum_{j=2}^r \sum_{i=0}^{r-j} \tilde{\alpha}_i^{j+r-1}} = \frac{1}{(\epsilon + I_k^n)^t} \frac{1}{\sum_{j=2}^r \sum_{i=0}^{r-j} \frac{1}{(\epsilon + I_i^{j+r-1})^t}}, \quad n = 4, 5,$$

339 where we are taking into account that the stencil has $2r$ points and $r = 3$.
 340 Replacing now $I_k^n = (h^2 f''_{j-1/2})^2 \cdot (1 + O(h^2))$, $n = 4, 5$, as shown in Theorem
 341 3.1, and taking ϵ small enough, we obtain

$$342 \quad \tilde{\omega}_k^r = \frac{(1 + O(h^2))^t}{3(1 + O(h^2))^t},$$

343 but $(1 + O(h^2))^t = 1 + O(h^2)$ and $\frac{1}{(1 + O(h^2))^t} = 1 + O(h^2)$, so,

$$344 \quad \tilde{\omega}_k^r = \frac{(1 + O(h^2))^t}{3(1 + O(h^2))^t} = \frac{1}{3}(1 + O(h^2)).$$

345 For the particular case $r = 3$, (3.14) transforms into,

$$(3.16) \quad (\tilde{C}_0^3, \tilde{C}_1^3, \tilde{C}_2^3) = \frac{1}{3} (1 + O(h^2)) (\mathbf{C}_0^4 + \mathbf{C}_0^5 + \mathbf{C}_1^4) = \mathbf{C}_0^5 + O(h^2) \\ = (C_0^3, C_1^3, C_2^3) + O(h^2),$$

347 that are the original optimal weights $C_k^r(j)$ in (2.6) and proposed in [14] plus
 348 a small perturbation that, as we will see in Theorem 3.2, does not affect
 349 the order of accuracy. Applying exactly the same process but to the WENO
 350 weights in (2.10), using as optimal weights those in (3.16) we obtain,

$$351 \quad \omega_k^r = \frac{\tilde{\alpha}_k^r}{\sum_{i=0}^{r-1} \tilde{\alpha}_i^r} = \frac{C_k^r + O(h^2)}{(\epsilon + I_k^r)^t} \frac{1}{\sum_{i=0}^{r-1} \frac{C_i^r + O(h^2)}{(\epsilon + I_i^r)^t}},$$

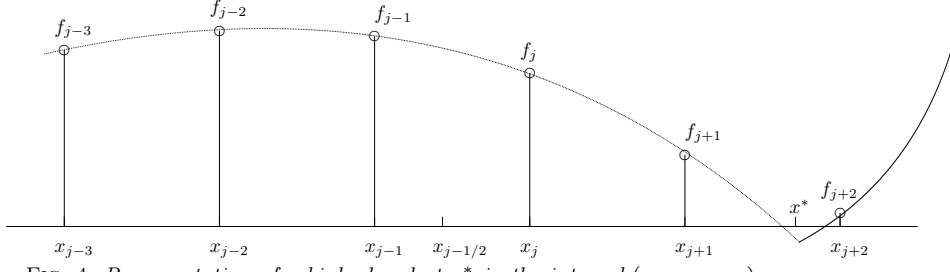
352 Replacing again the expression $I_k^r = I_i^r = (h^2 f''_{j-1/2})^2 \cdot (1 + O(h^2))$, for $r = 3$,
 353 and taking ϵ small enough, we obtain,

$$354 \quad (3.17) \quad \omega_k^r = \frac{C_k^r + O(h^2)}{(1 + O(h^2))^t} \frac{(1 + O(h^2))^t}{1 + O(h^2)} = C_k^r + O(h^2),$$

355 and the result is that the WENO weights are

$$356 \quad (3.18) \quad \omega_k^r = C_k^r + O(h^2)$$

357 • The cases shown in Figure 4 and 5 are symmetric, so we can just analyze the
 358 case presented in Figure 4. It is clear that a kink in the interval (x_{j+1}, x_{j+2})
 359 will produce that the smoothness indicators I_1^4 and I_0^5 shown in (3.5) and (3.6)
 360 respectively will take a value $O(h^2)$ due to the presence of the discontinuity

FIG. 4. Representation of a kink placed at x^* in the interval (x_{j+1}, x_{j+2}) .

361 in the first derivative, while $I_0^4 = (h^2 f''_{j-1/2})^2 \cdot (1 + O(h^2)) = O(h^4)$ as that
 362 part of the stencil is smooth. If that is the case, then

$$\begin{aligned} \tilde{\alpha}_0^4 &= \frac{1}{(\epsilon + O(h^4))^t}, \\ 363 \quad \tilde{\alpha}_0^5 &= \frac{1}{(\epsilon + O(h^2))^t}, \\ \tilde{\alpha}_1^4 &= \frac{1}{(\epsilon + O(h^2))^t}. \end{aligned}$$

364 Then we have that,

$$\tilde{w}_k^n = \frac{\tilde{\alpha}_k^n}{\sum_{j=2}^r \sum_{i=0}^{r-j} \tilde{\alpha}_i^{j+r-1}} = \frac{1}{(\epsilon + I_k^n)^t} \frac{1}{\sum_{j=2}^r \sum_{i=0}^{r-j} \frac{1}{(\epsilon + I_i^{j+r-1})^t}}, \quad n = 4, 5,$$

366 and $r = 3$. Assuming that ϵ is small enough, we obtain that the weights are,

$$\begin{aligned} \tilde{w}_0^4 &= \frac{1}{(\epsilon + I_0^4)^t} \frac{1}{\sum_{j=2}^r \sum_{i=0}^{r-j} \frac{1}{(\epsilon + I_i^{j+r-1})^t}} = \frac{1}{(\epsilon + I_0^4)^t} \frac{1}{\frac{1}{(\epsilon + I_0^4)^t} (1 + O(h^{2t}))} = \frac{1}{1 + O(h^{2t})} \\ &= 1 + O(h^{2t}), \\ 367 \quad \tilde{w}_1^4 &= \frac{1}{(\epsilon + I_1^4)^t} \frac{1}{\sum_{j=2}^r \sum_{i=0}^{r-j} \frac{1}{(\epsilon + I_i^{j+r-1})^t}} = \frac{1}{(\epsilon + I_1^4)^t} \frac{1}{\frac{1}{(\epsilon + I_0^4)^t} (1 + O(h^{2t}))} = O(h^{2t}), \\ \tilde{w}_0^5 &= \frac{1}{(\epsilon + I_0^5)^t} \frac{1}{\sum_{j=2}^r \sum_{i=0}^{r-j} \frac{1}{(\epsilon + I_i^{j+r-1})^t}} = \frac{1}{(\epsilon + I_0^5)^t} \frac{1}{\frac{1}{(\epsilon + I_0^4)^t} (1 + O(h^{2t}))} = O(h^{2t}). \end{aligned}$$

368 Then, the adapted optimal weights have the expression,

$$(3.19) \quad (\tilde{C}_0^3, \tilde{C}_1^3, \tilde{C}_2^3) = \mathbf{C}_0^4 + O(h^{2t}) = (2C_0^3, C_1^3, 0) + O(h^{2t}),$$

370 Exactly the same conclusions can be reached if a jump discontinuity in the
 371 function is found in the interval (x_{j+1}, x_{j+2}) . The only difference is that in

372 this case I_1^4 and I_0^5 are both $O(1)$ and,

$$\begin{aligned}
 \tilde{w}_0^4 &= \frac{1}{(\epsilon + I_0^4)^t} \frac{1}{\sum_{j=2}^r \sum_{i=0}^{r-j} \frac{1}{(\epsilon + I_i^{j+r-1})^t}} = \frac{1}{(\epsilon + I_0^4)^t} \frac{1}{\frac{1}{(\epsilon + I_0^4)^t} (1 + O(h^{4t}))} = \frac{1}{1 + O(h^{4t})} \\
 &= 1 + O(h^{4t}), \\
 \tilde{w}_1^4 &= \frac{1}{(\epsilon + I_1^5)^t} \frac{1}{\sum_{j=2}^r \sum_{i=0}^{r-j} \frac{1}{(\epsilon + I_i^{j+r-1})^t}} = \frac{1}{(\epsilon + I_1^4)^t} \frac{1}{\frac{1}{(\epsilon + I_0^4)^t} (1 + O(h^{4t}))} = O(h^{4t}), \\
 \tilde{w}_0^5 &= \frac{1}{(\epsilon + I_0^5)^t} \frac{1}{\sum_{j=2}^r \sum_{i=0}^{r-j} \frac{1}{(\epsilon + I_i^{j+r-1})^t}} = \frac{1}{(\epsilon + I_0^5)^t} \frac{1}{\frac{1}{(\epsilon + I_0^4)^t} (1 + O(h^{4t}))} = O(h^{4t}).
 \end{aligned}
 \tag{373}$$

374 Then, the adapted optimal weights have the expression,

$$\tag{375} \quad (\tilde{C}_0^3, \tilde{C}_1^3, \tilde{C}_2^3) = \mathbf{C}_0^4 + O(h^{4t}) = (2C_0^3, C_1^3, 0) + O(h^{4t}).$$

376 If the discontinuity is placed in the interval (x_{j-3}, x_{j-2}) , the conclusions
377 would be exactly the same but

$$\tag{378} \quad (\tilde{C}_0^3, \tilde{C}_1^3, \tilde{C}_2^3) = \mathbf{C}_1^4 + O(h^{2t}) = (0, C_1^3, 2C_2^3) + O(h^{2t}),$$

379 for a kink, or

$$\tag{380} \quad (\tilde{C}_0^3, \tilde{C}_1^3, \tilde{C}_2^3) = \mathbf{C}_1^4 + O(h^{4t}) = (0, C_1^3, 2C_2^3) + O(h^{4t}),$$

381 for a jump discontinuity.

382 Now, let's see what we obtain using WENO algorithm with these adapted
383 optimal weights instead of the original optimal weights (2.10). If there is a
384 kink in the interval (x_{j+1}, x_{j+2}) we know that $I_0^3 = O(h^4)$, $I_1^3 = O(h^4)$ and
385 $I_2^3 = O(h^2)$. If we assume that ϵ is small enough, we suppose that we have
386 obtained as nonlinear optimal weights $(\tilde{C}_0^3, \tilde{C}_1^3, \tilde{C}_2^3) = (2C_0^3, C_1^3, 0) + O(h^{2t})$
387 as shown in (3.19) and we take into account that, in this case, $\tilde{C}_0^3 + \tilde{C}_1^3 + \tilde{C}_2^3 =$
388 $2C_0^3 + C_1^3 + O(h^{2t}) = 1 + O(h^{2t})$, then,

$$\begin{aligned}
 \tag{3.23} \quad \omega_0^3 &= \frac{\tilde{C}_0^3}{(\epsilon + I_0^3)^t} \frac{1}{\sum_{i=0}^{r-1} \frac{\tilde{C}_i^3}{(\epsilon + I_i^3)^t}} = \frac{\tilde{C}_0^3}{(\epsilon + I_0^3)^t} \frac{1}{\frac{1}{(\epsilon + I_0^3)^t} (\tilde{C}_0^3 + \tilde{C}_1^3 (1 + O(h^2)) + O(h^{2t}))} \\
 &= \frac{\tilde{C}_0^3}{1 + O(h^2)} = \tilde{C}_0^3 + O(h^2),
 \end{aligned}$$

$$\begin{aligned}
\omega_1^3 &= \frac{\tilde{C}_1^3}{(\epsilon + I_1^3)^t} \sum_{i=0}^{r-1} \frac{1}{\tilde{C}_i^3} = \frac{\tilde{C}_1^3}{(\epsilon + I_1^3)^t} \frac{1}{\frac{1}{(\epsilon + I_1^3)^t} (\tilde{C}_0^3(1 + O(h^2)) + \tilde{C}_1^3 + O(h^{2t}))} \\
&= \frac{\tilde{C}_1^3}{1 + O(h^2)} = \tilde{C}_1^3 + O(h^2), \\
390 \quad \omega_2^3 &= \frac{\tilde{C}_2^3}{(\epsilon + I_2^3)^t} \sum_{i=0}^{r-1} \frac{1}{\tilde{C}_i^3} = \frac{\tilde{C}_2^3}{(\epsilon + I_2^3)^t} \frac{1}{\frac{1}{(\epsilon + I_0^3)^t} (\tilde{C}_0^3 + \tilde{C}_1^3(1 + O(h^2)) + O(h^{2t}))} \\
&= \frac{\tilde{C}_2^3}{O(h^{2t})} \frac{1}{\frac{1}{O(h^{4t})}(1 + O(h^2))} = O(h^{2t}).
\end{aligned}$$

If there is a jump, the analysis is analogous and

$$(3.24) \quad \omega_0^3 = \tilde{C}_0^3 + O(h^4), \quad \omega_1^3 = \tilde{C}_1^3 + O(h^4), \quad \omega_2^3 = O(h^{4t}).$$

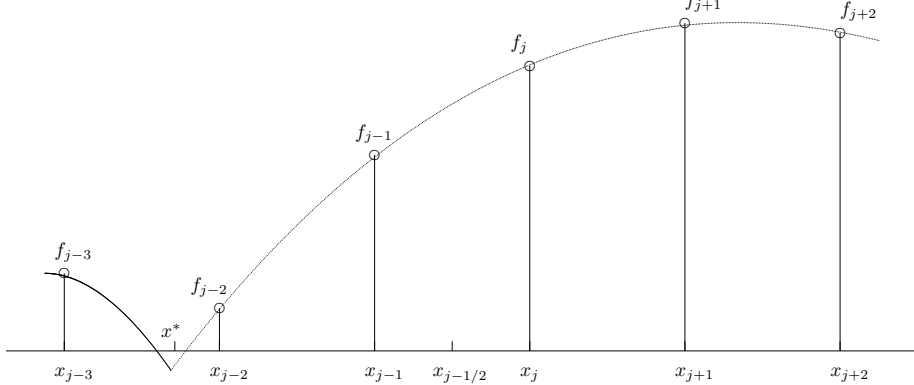


FIG. 5. Representation of a kink placed at x^* in the interval (x_{j-3}, x_{j-2}) .

- If there is a kink or a jump in the function affecting the stencil in the intervals (x_j, x_{j+1}) or (x_{j-2}, x_{j-1}) , there is no hope of attaining adaption through the modification of the optimal weights. The best order of accuracy that can be obtained is $O(h^4)$, the same as the classical WENO algorithm attains, as there is only one smooth stencil. In this case the adapted optimal weights (3.12) would be,

$$(3.25) \quad \tilde{\omega}_0^4 = O(1), \quad \tilde{\omega}_0^5 = O(1), \quad \tilde{\omega}_1^4 = O(1).$$

In this situation, basically it is WENO strategy who decides the weights for each polynomial in (2.2). Let's see how WENO algorithm will behave. Let's analyze the case when the discontinuity is placed in the interval (x_j, x_{j+1}) as the case when the discontinuity is in the interval (x_{j-2}, x_{j-1}) is symmetric. As we did before, we can apply the same process to the WENO weights in (2.10), using as optimal weights those in (3.25). We know that we obtain,

$$\omega_j^3 = \frac{\tilde{\alpha}_j^3}{\sum_{i=0}^{r-1} \tilde{\alpha}_i^3} = \frac{O(1)}{(\epsilon + I_j^3)^t} \frac{1}{\sum_{i=0}^{r-1} \frac{O(1)}{(\epsilon + I_i^3)^t}}, \quad j = 0, 1, 2,$$

407 and that $I_0^3 = O(h^4)$, $I_1^3 = O(h^2)$ and $I_2^3 = O(h^2)$. If we assume that ϵ is
 408 small enough, and we suppose that we have obtained as nonlinear optimal
 409 weights $(\tilde{C}_0^3, \tilde{C}_1^3, \tilde{C}_2^3)$ then,

$$\begin{aligned}
 (3.26) \quad \omega_0^3 &= \frac{\tilde{C}_0^3}{(\epsilon + I_0^3)^t} \frac{1}{\sum_{i=0}^{r-1} \frac{\tilde{C}_i^3}{(\epsilon + I_i^3)^t}} = \frac{\tilde{C}_0^3}{(\epsilon + I_0^3)^t} \frac{1}{\frac{\tilde{C}_0^3}{(\epsilon + I_0^3)^t} (1 + O(h^{2t}))} = 1 + O(h^{2t}), \\
 \omega_1^3 &= \frac{\tilde{C}_1^3}{(\epsilon + I_1^3)^t} \frac{1}{\sum_{i=0}^{r-1} \frac{\tilde{C}_i^3}{(\epsilon + I_i^3)^t}} = \frac{\tilde{C}_1^3}{(\epsilon + I_1^3)^t} \frac{1}{\frac{\tilde{C}_1^3}{(\epsilon + I_1^3)^t} (1 + O(h^{2t}))} \\
 &= \frac{\tilde{C}_1^3}{O(h^{2t})} \frac{1}{\frac{\tilde{C}_0^3}{O(h^{4t})} (1 + O(h^{2t}))} = O(h^{2t}), \\
 \omega_2^3 &= \frac{\tilde{C}_2^3}{(\epsilon + I_2^3)^t} \frac{1}{\sum_{i=0}^{r-1} \frac{\tilde{C}_i^3}{(\epsilon + I_i^3)^t}} = \frac{\tilde{C}_2^3}{(\epsilon + I_2^3)^t} \frac{1}{\frac{\tilde{C}_2^3}{(\epsilon + I_2^3)^t} (1 + O(h^{2t}))} \\
 &= \frac{\tilde{C}_2^3}{O(h^{2t})} \frac{1}{\frac{\tilde{C}_0^3}{O(h^{4t})} (1 + O(h^{2t}))} = O(h^{2t}),
 \end{aligned}$$

410 and the result is that the first stencil of WENO algorithm receives a weight
 411 that is very close to 1 while the others are close to 0. If there is a jump
 412 discontinuity in the interval (x_j, x_{j+1}) , the analysis is analogous and
 413

$$(3.27) \quad \omega_0^3 = 1 + O(h^{4t}), \quad \omega_1^3 = O(h^{4t}), \quad \omega_2^3 = O(h^{4t}).$$

414 • Using the the new algorithm, it is clear that the hypothetical situation presented in Figure 6 will result in a loss of accuracy when the discontinuity is placed at the central interval of the stencil.

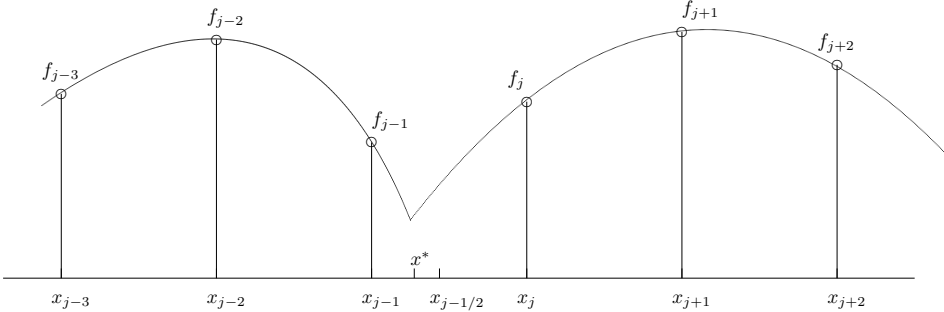


FIG. 6. Representation of a kink placed placed at x^* in the interval (x_{j-1}, x_j) .

417 Let's consider the stencil $S_r^{2r} = \{x_{j-3}, x_{j-2}, x_{j-1}, x_j, x_{j+1}, x_{j+2}\}$ and the point
 418 values $\{f_{j-3}, f_{j-2},$
 419 $f_{j-1}, f_j, f_{j+1}, f_{j+2}\}$. Now, we can prove the following theorem about the weights,
 420 that will also provide us information about the value of t and how small ϵ must be.
 421

422 THEOREM 3.2. Let's assume that $r = 3$, $t \geq 1$, $\epsilon \leq h^4$ and that the grid spacing
 423 h is small enough such that there is only one discontinuity in the considered stencil.
 424 In this situation we can take into account the four following situations:

- If the nonlinear optimal weights satisfy the following relation at smooth zones where,

$$(\tilde{C}_0^3, \tilde{C}_1^3, \tilde{C}_2^3) = \tilde{\omega}_0^4 \mathbf{C}_0^4 + \tilde{\omega}_0^5 \mathbf{C}_0^5 + \tilde{\omega}_1^4 \mathbf{C}_1^4 = \mathbf{C}_0^5 + O(h^2),$$

425 with $\mathbf{C}_0^5 = (C_0^3, C_1^3, C_2^3)$, then $\sum_{k=0}^{r-1} \omega_k^r p_k^r(x_{j-1/2}) = f(x_{j-1/2}) + O(h^6)$.

- If there is a discontinuity in the interval (x_{j-3}, x_{j-2}) and the nonlinear optimal weights satisfy the following relation,

$$(\tilde{C}_0^3, \tilde{C}_1^3, \tilde{C}_2^3) = \tilde{\omega}_0^4 \mathbf{C}_0^4 + \tilde{\omega}_0^5 \mathbf{C}_0^5 + \tilde{\omega}_1^4 \mathbf{C}_1^4 = \mathbf{C}_1^4 + O(h^2),$$

426 with $\mathbf{C}_1^4 = (0, C_1^3, 2C_2^3)$, then $\sum_{k=0}^{r-1} \omega_k^r p_k^r(x_{j-1/2}) = f(x_{j-1/2}) + O(h^5)$.

- If there is a discontinuity in the interval (x_{j+1}, x_{j+2}) and the nonlinear optimal weights satisfy the following relation,

$$(\tilde{C}_0^3, \tilde{C}_1^3, \tilde{C}_2^3) = \tilde{\omega}_0^4 \mathbf{C}_0^4 + \tilde{\omega}_0^5 \mathbf{C}_0^5 + \tilde{\omega}_1^4 \mathbf{C}_1^4 = \mathbf{C}_0^4 + O(h^2),$$

427 with $\mathbf{C}_0^4 = (2C_0^3, C_1^3, 0)$, then $\sum_{k=0}^{r-1} \omega_k^r p_k^r(x_{j-1/2}) = f(x_{j-1/2}) + O(h^5)$.

- If there is a discontinuity in the intervals (x_j, x_{j+1}) or (x_{j-2}, x_{j-1}) , then the nonlinear optimal weights satisfy the following relation,

$$(\tilde{C}_0^3, \tilde{C}_1^3, \tilde{C}_2^3) = \tilde{\omega}_0^4 \mathbf{C}_0^4 + \tilde{\omega}_0^5 \mathbf{C}_0^5 + \tilde{\omega}_1^4 \mathbf{C}_1^4 = (O(1), O(1), O(1)),$$

428 and $\sum_{k=0}^{r-1} \omega_k^r p_k^r(x_{j-1/2}) = f(x_{j-1/2}) + O(h^4)$.

429 *Proof.*

430

431 • Let's prove the first statement of the theorem. As shown in (3.9), the components of the vector \mathbf{C}_0^5 are the $C_k^r(j)$ in (2.7). We can start by writing the 432 error of interpolation obtained by the expression in (2.2) at $x_{j-1/2}$,

$$\begin{aligned} 434 \quad \sum_{k=0}^{r-1} \omega_k^r p_k^r(x_{j-1/2}) - f_{j-1/2} &= \sum_{k=0}^{r-1} \omega_k^r p_k^r(x_{j-1/2}) - f_{j-1/2} + \sum_{k=0}^{r-1} C_k^r p_k^r(x_{j-1/2}) \\ &\quad - \sum_{k=0}^{r-1} C_k^r p_k^r(x_{j-1/2}), \end{aligned}$$

435 where the C_k^r are the WENO optimal weights in (2.7). Grouping terms we 436 obtain,

$$\begin{aligned} 437 \quad \sum_{k=0}^{r-1} \omega_k^r p_k^r(x_{j-1/2}) - f_{j-1/2} &= \sum_{k=0}^{r-1} \omega_k^r p_k^r(x_{j-1/2}) - \sum_{k=0}^{r-1} C_k^r p_k^r(x_{j-1/2}) \\ &\quad + \sum_{k=0}^{r-1} C_k^r p_k^r(x_{j-1/2}) - f_{j-1/2} \\ &= \sum_{k=0}^{r-1} (\omega_k^r - C_k^r) p_k^r(x_{j-1/2}) + O(h^{2r}). \end{aligned}$$

438 And due to the fact that $\sum_{k=0}^{r-1} \omega_k^r = \sum_{k=0}^{r-1} C_k^r = 1$,

$$\begin{aligned}
 439 \quad & \sum_{k=0}^{r-1} \omega_k^r p_k^r(x_{j-1/2}) - f_{j-1/2} = \sum_{k=0}^{r-1} (\omega_k^r - C_k^r) p_k^r(x_{j-1/2}) + O(h^{2r}) \\
 & + \sum_{k=0}^{r-1} (\omega_k^r - C_k^r) f_{j-1/2} \\
 & = \sum_{k=0}^{r-1} (\omega_k^r - C_k^r) (p_k^r(x_{j-1/2}) - f_{j-1/2}) + O(h^{2r})
 \end{aligned}$$

440 From (3.17) it turns out that $(\omega_k^r - C_k^r) = O(h^m)$ with $m = 2$,

(3.28)

$$441 \quad \sum_{k=0}^{r-1} \omega_k^r p_k^r(x_{j-1/2}) - f_{j-1/2} = O(h^m) O(h^{r+1}) + O(h^{2r}) = O(h^{\min(m+r+1, 2r)}).$$

442 For the particular case $r = 3$, we obtain optimal accuracy $O(h^6)$ at smooth
443 zones.

444 • The second and third statements of the theorem are symmetric so let's prove
445 only the second statement. As shown in (3.8), $\mathbf{C}_1^4 = (0, C_1^3, 2C_2^3)$. We can
446 reproduce the proof in the previous point and write the error of interpolation
447 obtained in this case by the expression in (2.2) at $x_{j-1/2}$,

$$\begin{aligned}
 448 \quad & \sum_{k=0}^{r-1} \omega_k^r p_k^r(x_{j-1/2}) - f_{j-1/2} = \sum_{k=0}^{r-1} \omega_k^r p_k^r(x_{j-1/2}) - f_{j-1/2} + \sum_{k=0}^{r-1} \mathbf{C}_1^4(k) p_k^r(x_{j-1/2}) \\
 449 & - \sum_{k=0}^{r-1} \mathbf{C}_1^4(k) p_k^r(x_{j-1/2}),
 \end{aligned}$$

450 where the \mathbf{C}_1^4 are the WENO optimal weights that would provide $O(h^5)$
451 accuracy in this case, as shown in (3.8). Grouping terms we obtain,

$$\begin{aligned}
 452 \quad & \sum_{k=0}^{r-1} \omega_k^r p_k^r(x_{j-1/2}) - f_{j-1/2} = \sum_{k=0}^{r-1} \omega_k^r p_k^r(x_{j-1/2}) - \sum_{k=0}^{r-1} \mathbf{C}_1^4(k) p_k^r(x_{j-1/2}) \\
 & + \sum_{k=0}^{r-1} \mathbf{C}_1^4(k) p_k^r(x_{j-1/2}) - f_{j-1/2} \\
 & = \sum_{k=0}^{r-1} (\omega_k^r - \mathbf{C}_1^4(k)) p_k^r(x_{j-1/2}) + O(h^{2r-1}).
 \end{aligned}$$

453 And due to the fact that $\sum_{k=0}^{r-1} \omega_k^r = \sum_{k=0}^{r-1} \mathbf{C}_1^4(k) = 1$,

(3.29)

$$\begin{aligned}
 454 \quad & \sum_{k=0}^{r-1} \omega_k^r p_k^r(x_{j-1/2}) - f_{j-1/2} = \sum_{k=0}^{r-1} (\omega_k^r - \mathbf{C}_1^4(k)) (p_k^r(x_{j-1/2}) - f_{j-1/2}) + O(h^{2r-1}) \\
 & = O(h^m) O(h^{r+1}) + O(h^{2r-1}) = O(h^{\min(m+r+1, 2r-1)}),
 \end{aligned}$$

455 From (3.21) and (3.23), if $t \geq 1$, it turns out that if $(\omega_k^r - \mathbf{C}_1^4(k)) = O(h^m)$
456 with $m = 2$ for kinks and $m = 4$ for jumps. Thus, for the particular case

457 $r = 3$, we obtain optimal accuracy $O(h^5)$ for the situation presented in Figure
 458 5.

459 • The proof of the fourth statement of the theorem corresponds to the case
 460 when there is a discontinuity in the interval (x_j, x_{j+1}) or (x_{j-2}, x_{j-1}) . In this
 461 case there is only one smooth stencil of four points and WENO algorithm
 462 reaches the maximum accuracy without any modification. Lets consider the
 463 case analyzed in (3.26) when the discontinuity is in the interval (x_j, x_{j+1}) as
 464 the other case is symmetric. From (3.26) we can consider the vector $\mathbf{C} =$
 465 $(1, 0, 0)$. Following the same process as before, we have that,

$$466 \sum_{k=0}^{r-1} \omega_k^r p_k^r(x_{j-1/2}) - f_{j-1/2} = \sum_{k=0}^{r-1} \omega_k^r p_k^r(x_{j-1/2}) - f_{j-1/2} + \sum_{k=0}^{r-1} \mathbf{C}(k) p_k^r(x_{j-1/2}) \\ 467 - \sum_{k=0}^{r-1} \mathbf{C}(k) p_k^r(x_{j-1/2}),$$

468 Grouping terms we obtain,

$$469 \sum_{k=0}^{r-1} \omega_k^r p_k^r(x_{j-1/2}) - f_{j-1/2} = \sum_{k=0}^{r-1} \omega_k^r p_k^r(x_{j-1/2}) - \sum_{k=0}^{r-1} \mathbf{C}(k) p_k^r(x_{j-1/2}) \\ + \sum_{k=0}^{r-1} \mathbf{C}(k) p_k^r(x_{j-1/2}) - f_{j-1/2} \\ = \sum_{k=0}^{r-1} (\omega_k^r - \mathbf{C}(k)) p_k^r(x_{j-1/2}) + O(h^{r+1}).$$

470 And due to the fact that $\sum_{k=0}^{r-1} \omega_k^r = \sum_{k=0}^{r-1} \mathbf{C}(k) = 1$,
 (3.30)

$$471 \sum_{k=0}^{r-1} \omega_k^r p_k^r(x_{j-1/2}) - f_{j-1/2} = \sum_{k=0}^{r-1} (\omega_k^r - \mathbf{C}(k)) (p_k^r(x_{j-1/2}) - f_{j-1/2}) + O(h^{r+1}) \\ = O(h^m) O(h^{r+1}) + O(h^{r+1}) = O(h^{\min(m+r+1, r+1)}).$$

472 From (3.26) and (3.27) it is clear that $m = 2t$ for kinks and $m = 4t$ for jumps.
 473 Thus, for the particular case $r = 3$ with $t \geq 1$, we obtain optimal accuracy
 474 $O(h^4)$ if we find a discontinuity in the intervals (x_j, x_{j+1}) or (x_{j-2}, x_{j-1}) . \square

475 The previous theorem leads to the following corollary

476 **COROLLARY 3.3.** *Considering the initial hypothesis $r = 3$, $t \geq 1$, and $\epsilon \leq h^4$ the
 477 new WENO interpolant is at least as good as WENO interpolant close to discontinui-
 478 ties.*

479 *Proof.* The proof is straightforward from the hypothesis and the proof of previous
 480 theorem. It basically consists in comparing the order of accuracy that WENO would
 481 obtain with the accuracy that the new WENO method obtains. In order to do this,
 482 we can just follow the proof of the previous theorem:

483 • If there is no discontinuity affecting the stencil, for $r = 3$ WENO obtains
 484 $O(h^6)$ accuracy and from (3.28) the new WENO algorithm also obtains $O(h^6)$
 485 accuracy.

- If there is a discontinuity in the interval (x_{j-3}, x_{j-2}) or (x_{j+1}, x_{j+2}) , WENO algorithm typically obtains $O(h^4)$ accuracy. From (3.29) the new WENO algorithm obtains $O(h^5)$ accuracy with $t \geq 1$.
- If there is a discontinuity in the intervals (x_j, x_{j+1}) or (x_{j-2}, x_{j-1}) , WENO algorithm obtains $O(h^4)$ accuracy. From (3.30) the new WENO algorithm obtains $O(h^4)$ accuracy with $t \geq 1$.

A *small enough* value of ϵ in (3.13) and in (2.10) is a value of order $O(h^4)$, as this is the minimum value of the new smoothness indicators (3.4), (3.5) and (3.6), that is reached at smooth zones, as can be seen from Theorem 3.1. \square

3.3. Increasing the accuracy at the central interval of the stencil in the point values. In this subsection we will analyze how to increase the accuracy attained by WENO method when a kink is placed at the central interval of the stencil, as shown in Figure 6. It is important to remember that in the point value setting, the position of jump discontinuities is lost during the discretization process and we can not hope to localize their exact position [38]. In [1] we extend the algorithm presented in this article for working in the cell averages and to the solution of conservation laws. We can use the smoothness indicators of three points shown in (3.3) in order to detect the presence of a kink in the central interval of the big stencil. If we use these smoothness indicators and a kink is placed in the interval (x_{j-1}, x_j) , then the first substencil $S_{-1}^2 = \{x_{j-3}, x_{j-2}, x_{j-1}\}$ and the fourth substencil $S_2^2 = \{x_j, x_{j+1}, x_{j+2}\}$ are smooth and I_{-1}^2 and I_2^2 take a value that is $O(h^4)$, while the second and third stencils $S_0^2 = \{x_{j-2}, x_{j-1}, x_j\}$, $S_1^2 = \{x_{j-1}, x_j, x_{j+1}\}$ are not smooth so I_0^2 and I_1^2 take value that is $O(h^2)$. This is a hint that should lead us to think that there is a kink at the interval (x_{j-1}, x_j) . For isolated discontinuities, we will have the following cases:

- If there is not a discontinuity in the interval (x_{j-1}, x_j) , then I_{-1}^2, I_0^2, I_1^2 and I_2^2 are $O(h^4)$.
- If there is a discontinuity in the interval (x_{j-1}, x_j) , then I_{-1}^2 and I_2^2 are $O(h^4)$ and I_0^2 and I_1^2 are $O(h^2)$.
- If there is a discontinuity at x_{j-1} , then I_{-1}^2, I_1^2 and I_2^2 are $O(h^4)$ and I_0^2 is $O(h^2)$.
- If there is a discontinuity at x_j , then I_{-1}^2, I_0^2 and I_2^2 are $O(h^4)$ and I_1^2 is $O(h^2)$.

Our objective is to localize the position of the discontinuity and, depending on its position with respect to $x_{j-1/2}$, then extrapolate at $x_{j-1/2}$ using S_{-1}^2 or S_2^2 . This process is inspired by Harten's ENO subcell resolution algorithm. Due to the bigger errors associated to the extrapolation process we would like to use it only when it is strictly necessary. Moreover, the extrapolation process that we propose reduces the stencil in order to avoid the discontinuity and, hence, implies order reduction if the location process fails and detects a discontinuity at a smooth zone. Thus, we only want to apply it at real singularities.

Being h the grid spacing, when $h(I_0^2 + I_1^2) > I_{-1}^2 + I_2^2$ the interval (x_{j-1}, x_j) is considered suspicious of containing a discontinuity. In this case, we build the second order interpolating polynomial $p_0^2(x)$, using the data $\{f_{j-3}, f_{j-2}, f_{j-1}\}$, that corresponds to the stencil S_0^2 , and the second order interpolating polynomial $p_3^2(x)$, using the data $\{f_j, f_{j+1}, f_{j+2}\}$, that correspond to S_3^2 . Then we build the function $g(x) = p_0^2(x) - p_3^2(x)$. Supposing that there is only one zero of $g(x)$ inside the interval (x_{j-1}, x_j) , that zero corresponds to the position of the discontinuity with $O(h^3)$ accuracy. Even though, we do not need to find the zeros of $g(x)$ but only to know if one of them is placed in the interval $(x_{j-1}, x_{j-1/2})$ or in the interval $(x_{j-1/2}, x_j)$. Evaluating $g(x)$ at $x_{j-1}, x_{j-1/2}$ and x_j and using Bolzano's theorem we can know in which of the

535 previous subintervals we can find the discontinuity, if there is one. If the discontinuity
 536 is placed in the interval $(x_{j-1}, x_{j-1/2})$, we will use $p_3^2(x)$ to extrapolate at $x_{j-1/2}$ in
 537 order to obtain an $O(h^3)$ approximation. On the other hand, if the discontinuity is
 538 placed in the interval $(x_{j-1/2}, x_j)$, we will use $p_0^2(x)$ to extrapolate at $x_{j-1/2}$. This
 539 technique assures $O(h^3)$ accuracy when a kink is placed in the central interval of the
 540 stencil. This process is somewhat similar to the one described by Harten in [41] to
 541 construct ENO *subcell-resolution* algorithm for conservation laws. Of course, the grid
 542 must be fine enough so that the discontinuity can be detected. Thus, it must be a-
 543 ssured that the grid spacing is below a critical value h_c that guarantees the detection
 544 of the singularity. The smoothness indicators used in this work are based on second
 545 order differences, which are the base of the detection algorithm in [38]. As a conse-
 546 quence, the value of the critical grid spacing h_c can be directly taken from Section 4,
 547 Lemma 2 of [38]. The interested reader can refer to [38] for a deeper explanation of
 548 this point.

549 **3.4. ENO property.** It is important to remember that the technique presented
 550 in Section 3.2 or 3.3 is basically a WENO algorithm where we modify the original
 551 optimal weights in order to assure the maximum possible order close to discontinuities.

552 The new WENO technique assures that the resulting polynomial satisfies the
 553 following properties:

- 554 • It is a piecewise polynomial interpolation composed of polynomials of even
 555 degree r .
- 556 • Every polynomial must satisfy the so-called *essentially non-oscillatory property*, through the emulation of the ENO algorithm [14]:
 - 557 – If the function f is smooth at the stencil S_k^r , then the weight related to
 558 this stencil will verify $w_k^r = O(1)$.
 - 559 – If the function f has a singularity at the stencil S_k^r , then the correspon-
 560 ding w_k^r will verify $w_k^r \leq O(h^r)$.

561 If the weights w_k^r that appear in (2.3) are designed to satisfy the ENO property, then
 562 $q_{j-r}(x)$ in (2.2) is a nonlinear convex combination of polynomials built using smooth
 563 stencils and where the contribution of stencils crossing discontinuities is negligible.

564 **THEOREM 3.4.** *The new algorithm satisfies the ENO property for $t \geq 2$, satisfying
 565 at the same time Theorem 3.2.*

566 *Proof.* For $t \geq 1$ Theorem 3.2 is satisfied, so for $t \geq 2$ it is also satisfied. From
 567 (3.18), (3.23) and (3.26) we can see that for $t \geq 2$:

- 568 • If the function f is smooth at the stencil S_k^r , then the weight related to this
 569 stencil will verify $w_k^r = O(1)$.
- 570 • If the function f has a singularity at the stencil S_k^r , then the corresponding
 571 w_k^r will verify $w_k^r \leq O(h^r)$.

572 This is precisely the ENO property. □

574 **4. Numerical experiments.** In this section we have used the functions plotted
 575 in Figure 7 and presented in (4.1), (4.2) and (4.3). The function in (4.1) is a piecewise
 576 polynomial of degree eight. The function in (4.2) is the product of two sinusoidal
 577 functions plus a polynomial. The function in (4.3) presents a jump discontinuity.
 578 We have used a stencil of six points, i.e. $r = 3$ in (2.1), so no one of the functions
 579 proposed can be interpolated exactly. Following Corollary 3.3 and Subsection 3.4,
 580 we have chosen the parameters $t = 2$ and $\epsilon \leq h^4$ for the new algorithm shown in
 581 Subsection 3.2. For WENO it is enough to choose $t = 2$ and $\epsilon \leq h^2$, as shown in [15].
 582 We have used in all the experiments the smoothness indicators proposed in (3.1).

583 In all the experiments presented, in order to obtain lower resolution versions of
 584 the initial data, we start from a discretized version at a higher resolution and then
 585 we take one of every 2^n samples. Using interpolation we recover a high resolution
 586 approximation of the original data. We have chosen to interpolate at the odd knots.

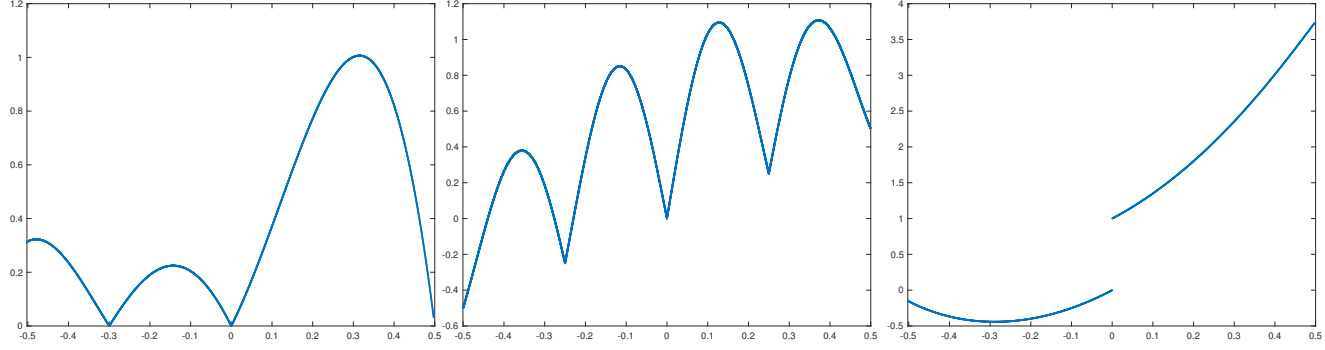


FIG. 7. In this figure we represent the functions (4.1), (4.2) and (4.3) that will be used for the numerical experiments of this section.

587 **Example 1** Let's start with the function plotted in Figure (7) to the left,

588 (4.1) $f(x) = |(x - 3)(x - 1.5)(x - 0.5)(x + \eta)(x + 0.3)(x + 0.6)(x + 5)(x + 1.5)|,$

589 for $-0.5 - \xi \leq x < 0.5 - \xi$. Setting grid spacing to $h_i = \frac{1}{2^i}, i = 6, 7, \dots, 12$, we
 590 check the accuracy of the interpolation through a grid refinement analysis close to the
 591 discontinuity at $x = 0$. In order to obtain the error, we compare with the function
 592 discretized with $h_{i+1} = \frac{1}{2^{i+1}}$. The worst case is when the discontinuity does not fall
 593 in a grid point (otherwise, there is always a smooth stencil). In order to assure the
 594 worse case for all the discretizations used, we place the discontinuity around which
 595 we will do the grid refinement analysis at $x = -\eta$, with $\eta = (2/3)h_{13}$ and we place
 596 the left side of the interval at $x = -0.5 - \xi$ with $\xi = 10h_{13}$. These considerations are
 597 only taken for doing the grid refinement analysis and would not be necessary in a real
 598 application of the algorithm.

599 We consider the errors at the nodes $\{x_{2j-6}, x_{2j-4}, x_{2j-2}, x_{2j}, x_{2j+2}, x_{2j+4}, x_{2j+6}\}$,
 600 being x_{2j} the prediction at the interval that contains the discontinuity (in this first
 601 experiment close to $x = 0$). Table 1 shows the results obtained by WENO algorithm
 602 using the smoothness indicator proposed in (3.1) and whose expressions are shown
 603 in (3.4). Table 2 shows the results obtained at the same points for the new optimal
 604 weights, described in Subsection 3.2, and WENO. The two tables show the order of
 605 accuracy between the successive errors when refining the grid. We can see how the
 606 accuracy is lost by both algorithms at the interval that contains the discontinuity.
 607 Also, as explained in Subsection 3.2, WENO is designed to obtain optimal order at
 608 smooth zones and to eliminate spurious oscillations close to discontinuities, but not
 609 optimizing the order in this last case. This fact can be seen in Table 1 at x_{2j-4} and
 610 x_{2j+4} . In both cases there are two smooth stencils, containing in total 5 points be-
 611 longing to the same side of the singularity. This means that the maximum theoretical
 612 accuracy that can be obtained is $O(h^5)$ and WENO algorithm obtains $O(h^4)$. As it
 613 can be analyzed in Table 2, using the new optimal weights presented in Subsection
 614 3.2, we attain the maximum theoretical accuracy in the whole interval except at the

interval that contains the singularity. Table 3 shows the results obtained by the new algorithm proposed in Subsection 3.3. We can see how the algorithm reproduces the behavior of the algorithm presented in Subsection 3.2 in terms of accuracy, at the intervals that are close to the discontinuity but do not contain it. At the interval that contains the discontinuity we have managed to raise the accuracy using the strategy inspired by ENO-Subcell resolution algorithm that was presented in Subsection 3.3. Figure 8 shows the absolute error distribution for the three algorithms when interpolating the function in (4.1) using $2^{12} = 4096$ samples. To the left we can see the error obtained by WENO algorithm, at the center the error obtained using the new weights presented in Subsection 3.2 and to the right the error obtained by the new algorithm presented in Subsection 3.3. We can see how the error presented in this last plot is six orders of magnitude smaller than in the other two plots.

i	x_{2j-6}		x_{2j-4}		x_{2j-2}		x_{2j}		x_{2j+2}		x_{2j+4}		x_{2j+6}	
	e_i	$\log_2 \left(\frac{e_i}{e_{i+1}} \right)$	e_i	$\log_2 \left(\frac{e_i}{e_{i+1}} \right)$	e_i	$\log_2 \left(\frac{e_i}{e_{i+1}} \right)$	e_i	$\log_2 \left(\frac{e_i}{e_{i+1}} \right)$	e_i	$\log_2 \left(\frac{e_i}{e_{i+1}} \right)$	e_i	$\log_2 \left(\frac{e_i}{e_{i+1}} \right)$	e_i	$\log_2 \left(\frac{e_i}{e_{i+1}} \right)$
6	1.848e-08	-	4.867e-07	-	2.031e-06	-	1.076e-03	-	5.188e-05	1.475e-05	2.299e-08	-	-	-
7	2.943e-10	5.973	2.972e-08	4.034	1.271e-07	3.998	1.075e-03	0.001	1.771e-06	4.873	2.325e-07	5.988	3.274e-10	6.133
8	4.668e-12	5.978	1.843e-09	4.011	7.934e-09	4.002	1.052e-03	0.032	1.901e-08	6.542	2.696e-09	6.430	4.914e-12	6.058
9	7.359e-14	5.987	1.148e-10	4.005	4.941e-10	4.005	1.017e-03	0.048	5.484e-10	5.115	1.178e-10	4.516	7.546e-14	6.025
10	1.154e-15	5.995	7.141e-12	4.007	2.974e-11	4.054	8.539e-04	0.253	3.132e-11	4.130	7.171e-12	4.038	1.171e-15	6.010
11	1.908e-17	5.918	4.482e-13	3.994	1.941e-12	3.938	1.491e-04	2.518	2.220e-12	3.818	4.673e-13	3.940	1.735e-17	6.077
12	0	-	2.800e-14	4.000	1.212e-13	4.001	1.532e-04	-0.039	1.227e-13	4.177	2.806e-14	4.058	1.301e-18	3.737

TABLE 1

Grid refinement analysis for the smoothness indicators presented in (3.1) and WENO algorithm for the function in (4.1). We can see how the accuracy is reduced at the interval that contains the singularity and around it. At x_{2j-4} and x_{2j+4} there is enough information to obtain $O(h^5)$ accuracy, but WENO is not designed to optimize the accuracy close to the discontinuities.

i	x_{2j-6}		x_{2j-4}		x_{2j-2}		x_{2j}		x_{2j+2}		x_{2j+4}		x_{2j+6}	
	e_i	$\log_2 \left(\frac{e_i}{e_{i+1}} \right)$	e_i	$\log_2 \left(\frac{e_i}{e_{i+1}} \right)$	e_i	$\log_2 \left(\frac{e_i}{e_{i+1}} \right)$	e_i	$\log_2 \left(\frac{e_i}{e_{i+1}} \right)$	e_i	$\log_2 \left(\frac{e_i}{e_{i+1}} \right)$	e_i	$\log_2 \left(\frac{e_i}{e_{i+1}} \right)$	e_i	$\log_2 \left(\frac{e_i}{e_{i+1}} \right)$
6	1.848e-08	-	6.681e-09	-	2.052e-06	-	1.076e-03	-	3.048e-05	-	1.084e-05	-	2.299e-08	-
7	2.943e-10	5.973	1.240e-10	5.751	1.278e-07	4.005	1.077e-03	-0.000	9.762e-07	4.964	3.377e-08	8.326	3.275e-10	6.133
8	4.668e-12	5.978	9.334e-12	3.732	7.961e-09	4.005	1.062e-03	0.020	1.457e-08	6.066	5.100e-11	9.371	4.914e-12	6.058
9	7.359e-14	5.987	3.789e-13	4.623	4.956e-10	4.006	1.034e-03	0.039	5.593e-10	4.703	6.597e-13	6.272	7.546e-14	6.025
10	1.154e-15	5.995	1.294e-14	4.872	2.952e-11	4.069	8.537e-04	0.276	3.125e-11	4.162	1.677e-14	5.298	1.171e-15	6.010
11	1.908e-17	5.918	4.454e-16	4.861	1.942e-12	3.926	1.511e-04	2.499	2.121e-12	3.881	5.594e-16	4.906	1.735e-17	6.077
12	0	-	1.409e-17	4.982	1.213e-13	4.001	1.540e-04	-0.028	1.232e-13	4.106	1.518e-17	5.204	8.674e-19	4.322

TABLE 2

Grid refinement analysis for the new optimal weights presented in Subsection 3.2 and WENO algorithm for the function in (4.1). We can see how the accuracy is lost at the interval that contains the singularity, but it is controlled close to it, decreasing step by step as we move towards the singularity.

i	x_{2j-6}		x_{2j-4}		x_{2j-2}		x_{2j}		x_{2j+2}		x_{2j+4}		x_{2j+6}	
	e_i	$\log_2 \left(\frac{e_i}{e_{i+1}} \right)$	e_i	$\log_2 \left(\frac{e_i}{e_{i+1}} \right)$	e_i	$\log_2 \left(\frac{e_i}{e_{i+1}} \right)$	e_i	$\log_2 \left(\frac{e_i}{e_{i+1}} \right)$	e_i	$\log_2 \left(\frac{e_i}{e_{i+1}} \right)$	e_i	$\log_2 \left(\frac{e_i}{e_{i+1}} \right)$	e_i	$\log_2 \left(\frac{e_i}{e_{i+1}} \right)$
6	1.848e-08	-	6.681e-09	-	8.870e-05	-	1.416e-04	-	3.048e-05	-	1.084e-05	-	2.299e-08	-
7	2.943e-10	5.973	1.240e-10	5.751	1.278e-07	9.439	1.610e-05	3.136	9.762e-07	4.964	3.377e-08	8.326	3.275e-10	6.133
8	4.668e-12	5.978	9.334e-12	3.732	7.961e-09	4.005	1.911e-06	3.075	1.457e-08	6.066	5.100e-11	9.371	4.914e-12	6.058
9	7.359e-14	5.987	3.789e-13	4.623	4.956e-10	4.006	2.320e-07	3.039	5.593e-10	4.703	6.597e-13	6.272	7.546e-14	6.025
10	1.154e-15	5.995	1.294e-14	4.872	2.952e-11	4.069	2.810e-08	3.049	3.125e-11	4.162	1.677e-14	5.298	1.171e-15	6.010
11	1.908e-17	5.918	4.454e-16	4.861	1.942e-12	3.926	3.573e-09	2.975	2.121e-12	3.881	5.594e-16	4.906	1.735e-17	6.077
12	0	-	1.409e-17	4.982	1.213e-13	4.001	4.450e-10	3.005	1.232e-13	4.106	1.518e-17	5.204	8.674e-19	4.322

TABLE 3

Grid refinement analysis for the algorithm presented in Subsection 3.3 for the function in (4.1). We can see how the accuracy is raised at the interval that contains the singularity and how the order decreases in a controlled way, step by step as we move towards the singularity.

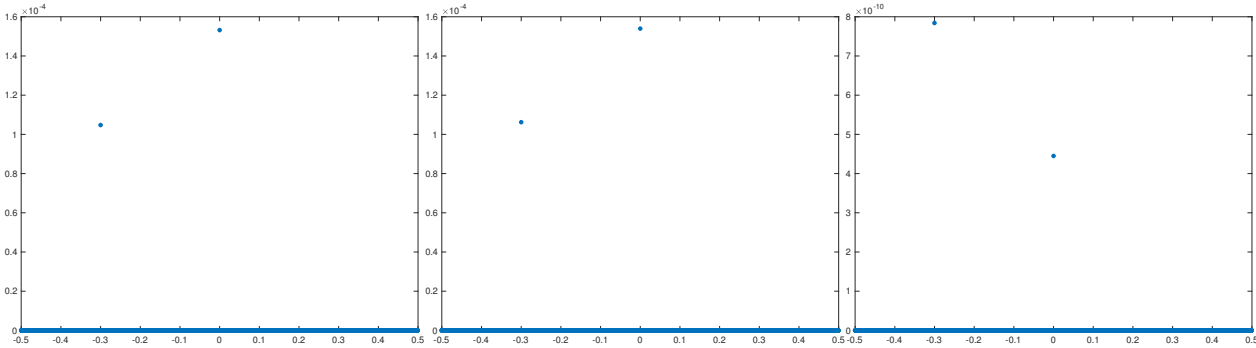


FIG. 8. Absolute error obtained when reconstructing the function in (4.1) through WENO (left), through the algorithm presented in Subsection 3.2 (center) and through the algorithm presented in Subsection 3.3 (right). The original data was 8192 points and the subsampled data was 4096 points.

627 **Example 2** Let's continue with the function plotted in Figure (7) at the center,

628 (4.2)
$$l(x) = |\sin(4\pi(x + \eta))| \cos((2(x + \eta)) + x), \quad -0.5 - \xi \leq x < 0.5 - \xi.$$

629 As before, we set $h_i = \frac{1}{2^i}, i = 6, 7, \dots, 12$, in order to check the accuracy of the
630 interpolation through a grid refinement analysis close to the singularity that is placed
631 in the interval $(-0.3, -0.2)$. As before, in order to obtain the error we compare with
632 the function discretized with $h_{i+1} = \frac{1}{2^{i+1}}$. As mentioned in the previous experiment,
633 in order to assure that the singularities do not fall at a grid point, we shift the
634 function by $\eta = (2/3)h_{13}$ and we place the left side of the interval at $x = -0.5 - \xi$
635 with $\xi = 3h_{13}$. Table 4 shows a grid refinement analysis for the results of WENO
636 algorithm at the singularity placed in the interval $(-0.2, -0.3)$ of function in (4.2).
637 The conclusions that we can reach for this experiment are the same as those we
638 obtained for the previous experiment. We can clearly observe how the accuracy is
639 reduced around the interval that contains the singularity, but not in an optimal way.
640 Table 5 shows the results obtained for the same function but using WENO with the
641 new weights introduced in Subsection 3.2. We can see that the accuracy also decreases
642 around the central interval but, in this case, reducing the order one step at a time
643 as we proceed towards the singularity. Table 6 shows the results obtained using the
644 new algorithm introduced in Subsection 3.3. We can see that the order of accuracy
645 is optimal, including the interval that contains the singularity. Figure 9 shows the
646 absolute error distribution for the three algorithms when interpolating the function
647 in (4.2) using 2^{12} samples. As before, we can see how the error presented in the plot
648 to the right is several orders of magnitude smaller than the ones to the left and at the
649 center.

650 **Example 3** Let's finish with the function plotted in Figure (7) to the right,

651 (4.3)
$$f(x) = \begin{cases} -4x^7 + x^4 + 5x^2 + 3x, & 0.5 \leq x < 0, \\ -8x^7 + x^4 + 5x^2 + 3x + 1, & 0 \leq x < 0.5, \end{cases}$$

652 In this case we have set again $h_i = \frac{1}{2^i}, i = 7, 8, 9 \dots 11$, for the grid refinement analysis.
653 The function in (4.3) only presents a jump discontinuity that is placed at $x = 0$. Table
654 7 shows a grid refinement analysis for the results obtained using the WENO algorithm.
655 Table 8 shows the result obtained using the optimal weights presented in Subsection
656 3.2. In this case, the algorithm presented in Subsection 3.3 can not be applied, as the

i	x_{2j-6}		x_{2j-4}		x_{2j-2}		x_{2j}		x_{2j+2}		x_{2j+4}		x_{2j+6}	
	e_i	$\log_2\left(\frac{e_i}{e_{i+1}}\right)$	e_i	$\log_2\left(\frac{e_i}{e_{i+1}}\right)$	e_i	$\log_2\left(\frac{e_i}{e_{i+1}}\right)$	e_i	$\log_2\left(\frac{e_i}{e_{i+1}}\right)$	e_i	$\log_2\left(\frac{e_i}{e_{i+1}}\right)$	e_i	$\log_2\left(\frac{e_i}{e_{i+1}}\right)$	e_i	$\log_2\left(\frac{e_i}{e_{i+1}}\right)$
6	1.812e-06	-	6.743e-06	-	3.322e-05	-	9.801e-04	-	1.064e-04	-	1.735e-05	-	6.014e-07	-
7	2.312e-08	6.292	3.354e-07	4.329	1.634e-06	4.346	9.807e-04	-0.001	1.591e-06	6.063	3.142e-07	5.787	2.348e-10	11.322
8	3.274e-10	6.142	1.862e-08	4.171	8.709e-08	4.230	9.810e-04	-0.000	5.206e-08	4.934	1.198e-08	4.713	1.553e-10	0.596
9	4.889e-12	6.065	1.095e-09	4.088	4.958e-09	4.135	9.790e-04	0.003	3.677e-09	3.824	8.862e-10	3.756	3.753e-12	5.371
10	7.441e-14	6.038	6.637e-11	4.044	2.945e-10	4.073	9.591e-04	0.030	2.520e-10	3.867	5.976e-11	3.890	6.881e-14	5.770
11	1.027e-15	6.179	4.086e-12	4.022	1.792e-11	4.038	9.232e-04	0.055	1.658e-11	3.926	3.878e-12	3.946	1.443e-15	5.575
12	1.388e-16	2.888	2.537e-13	4.010	1.105e-12	4.019	7.755e-04	0.251	1.063e-12	3.963	2.467e-13	3.974	1.388e-16	3.379

TABLE 4

Grid refinement analysis for the smoothness indicators presented in (3.1) and WENO algorithm for the function in (4.2). We can see how the accuracy is reduced at the interval that contains the singularity and around it. At x_{2j-4} and x_{2j+4} there is enough information to obtain $O(h^5)$ accuracy, but WENO is not designed to optimize the accuracy close to the singularities.

i	x_{2j-6}		x_{2j-4}		x_{2j-2}		x_{2j}		x_{2j+2}		x_{2j+4}		x_{2j+6}	
	e_i	$\log_2\left(\frac{e_i}{e_{i+1}}\right)$	e_i	$\log_2\left(\frac{e_i}{e_{i+1}}\right)$	e_i	$\log_2\left(\frac{e_i}{e_{i+1}}\right)$	e_i	$\log_2\left(\frac{e_i}{e_{i+1}}\right)$	e_i	$\log_2\left(\frac{e_i}{e_{i+1}}\right)$	e_i	$\log_2\left(\frac{e_i}{e_{i+1}}\right)$	e_i	$\log_2\left(\frac{e_i}{e_{i+1}}\right)$
6	1.815e-06	-	2.339e-06	-	3.324e-05	-	9.801e-04	-	7.058e-05	-	1.682e-05	-	6.092e-07	-
7	2.315e-08	6.293	9.660e-08	4.598	1.634e-06	4.346	9.808e-04	-0.001	9.005e-07	6.292	1.722e-07	6.610	1.660e-10	11.842
8	3.275e-10	6.143	3.324e-09	4.861	8.709e-08	4.230	9.812e-04	-0.001	4.733e-08	4.250	4.230e-09	5.347	1.556e-10	0.093
9	4.890e-12	6.066	1.090e-10	4.930	4.958e-09	4.135	9.793e-04	0.002	3.626e-09	3.706	1.241e-10	5.091	3.756e-12	5.372
10	7.438e-14	6.039	3.496e-12	4.963	2.945e-10	4.073	9.672e-04	0.019	2.517e-10	3.848	3.725e-12	5.058	6.881e-14	5.771
11	1.027e-15	6.179	1.107e-13	4.981	1.792e-11	4.038	9.386e-04	0.043	1.658e-11	3.924	1.143e-13	5.027	1.443e-15	5.575
12	1.943e-16	2.402	3.192e-15	5.116	1.105e-12	4.020	7.753e-04	0.276	1.063e-12	3.963	3.358e-15	5.089	1.388e-16	3.379

TABLE 5

Grid refinement analysis for the new optimal weights presented in Subsection 3.2 and WENO algorithm for the function in (4.2). We can see how the accuracy is lost at the interval that contains the singularity, but it is controlled close to it, decreasing step by step as we move towards the singularity.

i	x_{2j-6}		x_{2j-4}		x_{2j-2}		x_{2j}		x_{2j+2}		x_{2j+4}		x_{2j+6}	
	e_i	$\log_2\left(\frac{e_i}{e_{i+1}}\right)$	e_i	$\log_2\left(\frac{e_i}{e_{i+1}}\right)$	e_i	$\log_2\left(\frac{e_i}{e_{i+1}}\right)$	e_i	$\log_2\left(\frac{e_i}{e_{i+1}}\right)$	e_i	$\log_2\left(\frac{e_i}{e_{i+1}}\right)$	e_i	$\log_2\left(\frac{e_i}{e_{i+1}}\right)$	e_i	$\log_2\left(\frac{e_i}{e_{i+1}}\right)$
6	1.815e-06	-	2.339e-06	-	1.862e-03	-	2.322e-03	-	7.058e-05	-	1.682e-05	-	6.092e-07	-
7	2.315e-08	6.293	9.660e-08	4.598	2.599e-04	2.841	2.894e-04	3.005	9.005e-07	6.292	1.722e-07	6.610	1.660e-10	11.842
8	3.275e-10	6.143	3.324e-09	4.861	3.382e-05	2.942	3.567e-05	3.020	4.733e-08	4.250	4.230e-09	5.347	1.556e-10	0.093
9	4.890e-12	6.066	1.090e-10	4.930	4.958e-09	12.736	4.414e-06	3.015	3.626e-09	3.706	1.241e-10	5.091	3.756e-12	5.372
10	7.438e-14	6.039	3.496e-12	4.963	2.945e-10	4.073	5.485e-07	3.008	2.517e-10	3.848	3.725e-12	5.058	6.881e-14	5.771
11	1.027e-15	6.179	1.107e-13	4.981	1.792e-11	4.038	6.835e-08	3.005	1.658e-11	3.924	1.143e-13	5.027	1.443e-15	5.575
12	1.943e-16	2.402	3.192e-15	5.116	1.105e-12	4.020	7.510e-09	3.006	1.063e-12	3.963	3.358e-15	5.089	1.388e-16	3.379

TABLE 6

Grid refinement analysis for the algorithm presented in Subsection 3.3 for the function in (4.2). We can see how the accuracy is raised at the interval that contains the singularity and how the order decreases in a controlled way, step by step as we move towards the singularity.

657 position of the jump discontinuity has been lost in the discretization process [38]. We
658 can see how the new optimal weights allow to control the reduction of accuracy close
659 to the discontinuity.

i	x_{2j-6}		x_{2j-4}		x_{2j-2}		x_{2j}		x_{2j+2}		x_{2j+4}		x_{2j+6}	
	e_i	$\log_2\left(\frac{e_i}{e_{i+1}}\right)$	e_i	$\log_2\left(\frac{e_i}{e_{i+1}}\right)$	e_i	$\log_2\left(\frac{e_i}{e_{i+1}}\right)$	e_i	$\log_2\left(\frac{e_i}{e_{i+1}}\right)$	e_i	$\log_2\left(\frac{e_i}{e_{i+1}}\right)$	e_i	$\log_2\left(\frac{e_i}{e_{i+1}}\right)$	e_i	$\log_2\left(\frac{e_i}{e_{i+1}}\right)$
6	8.073e-11	-	1.284e-08	-	5.596e-08	-	4.996e-01	-	5.508e-08	-	1.294e-08	-	1.349e-10	-
7	8.178e-13	6.625	8.054e-10	3.995	3.493e-09	4.002	4.999e-01	-0.001	3.486e-09	3.982	8.061e-10	4.004	8.493e-13	7.311
8	9.354e-15	6.450	5.037e-11	3.999	2.183e-10	4.000	5.000e-01	-0.000	2.182e-10	3.998	5.037e-11	4.000	3.775e-15	7.814
9	1.197e-16	6.288	3.148e-12	4.000	1.364e-11	4.000	5.000e-01	-0.000	1.364e-11	4.000	3.148e-12	4.000	2.220e-16	4.087
10	0	-	1.968e-13	4.000	8.527e-13	4.000	5.000e-01	-0.000	8.527e-13	4.000	1.970e-13	3.999	0	-
11	0	-	1.230e-14	4.000	5.329e-14	4.000	5.000e-01	-0.000	5.329e-14	4.000	1.243e-14	3.985	0	-
12	0	-	7.685e-16	4.000	3.331e-15	4.000	5.000e-01	-0.000	3.331e-15	4.000	6.661e-16	4.222	2.220e-16	-

TABLE 7

Grid refinement analysis for the smoothness indicator proposed in (3.1) and WENO algorithm for the function in (4.3). We can see how the accuracy is reduced at the central interval of the stencil and around it.

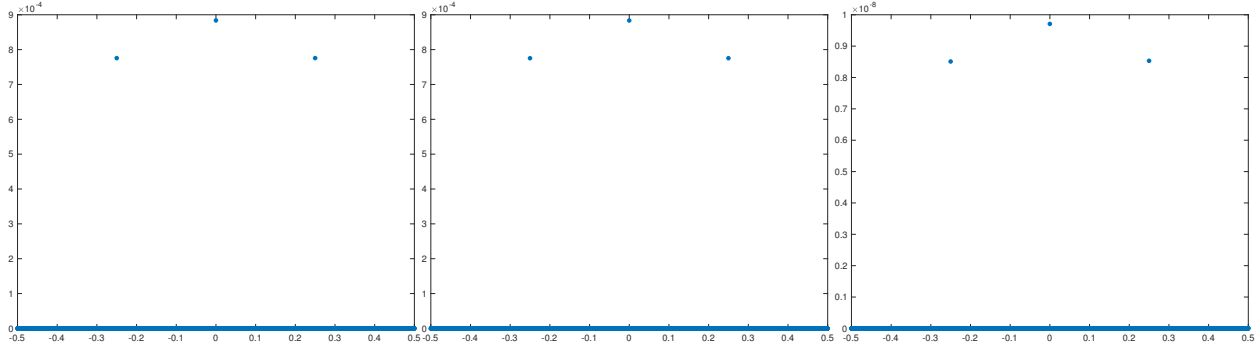


FIG. 9. Absolute error obtained when reconstructing the function in (4.2) through WENO (left), through the algorithm presented in Subsection 3.2 (center) and through the algorithm presented in Subsection 3.3 (right). The original data was 2^{13} points and the subsampled data was 2^{12} points.

i	x_{2j-6}		x_{2j-4}		x_{2j-2}		x_{2j}		x_{2j+2}		x_{2j+4}		x_{2j+6}	
	e_i	$\log_2\left(\frac{e_i}{e_{i+1}}\right)$	e_i	$\log_2\left(\frac{e_i}{e_{i+1}}\right)$	e_i	$\log_2\left(\frac{e_i}{e_{i+1}}\right)$	e_i	$\log_2\left(\frac{e_i}{e_{i+1}}\right)$	e_i	$\log_2\left(\frac{e_i}{e_{i+1}}\right)$	e_i	$\log_2\left(\frac{e_i}{e_{i+1}}\right)$	e_i	$\log_2\left(\frac{e_i}{e_{i+1}}\right)$
6	8.073e-11	-	1.295e-10	-	5.597e-08	-	4.996e-01	-	5.507e-08	-	4.475e-10	-	1.349e-10	-
7	8.178e-13	6.625	1.201e-12	6.753	3.493e-09	4.002	4.999e-01	-0.001	3.486e-09	3.982	3.296e-12	7.085	8.493e-13	7.311
8	9.354e-15	6.450	1.235e-14	6.603	2.183e-10	4.000	5.000e-01	-0.000	2.182e-10	3.998	2.287e-14	7.171	3.775e-15	7.814
9	1.162e-16	6.331	1.440e-16	6.423	1.364e-11	4.000	5.000e-01	-0.000	1.364e-11	4.000	2.220e-16	6.687	2.220e-16	4.087
10	1.735e-18	6.066	1.735e-18	6.375	8.527e-13	4.000	5.000e-01	-0.000	8.527e-13	4.000	0	-	0	-
11	0	-	0	-	5.329e-14	4.000	5.000e-01	-0.000	5.329e-14	4.000	0	-	0	-
12	0	-	0	-	3.331e-15	4.000	5.000e-01	-0.000	3.331e-15	4.000	2.220e-16	-	0	-

TABLE 8

Grid refinement analysis for the new optimal weights and WENO algorithm for the function in (4.3). We can see how the accuracy is increased around the discontinuity.

660 **Example 4** In this experiment we would like to check the computational performance
661 of the new algorithms compared to the classical WENO algorithm. The code
662 has been written in Matlab R2017b and executed in a laptop running OSX version
663 10.9.5 with a microprocessor Intel Core i5, 1.4GHz and 8 GB of RAM memory. In Ta-
664 ble 9 we present the results. In order to obtain each result presented in the table, we
665 have executed 50 times each algorithm with the same initial data, we have obtained
666 the computational time using the tic-toc buil-tin routines of Matlab and then we have
667 obtained the mean of the 50 results. The initial data have been the same as the one
668 used in the Examples 1, 2 and 3 at the same resolution used in the grid refinement
669 analysis presented. The conclusions that we can reach from these experiments is that
670 the new algorithms proposed are more expensive than the classical WENO, but not
671 so much. Comparing the two new algorithms presented in this paper, both behave
672 approximately the same in terms of computational time.

673 **5. Conclusions.** In this article we have presented and analyzed two strategies
674 that allow to improve the results obtained by WENO algorithm. The first one consists
675 in a new nonlinear design of the WENO optimal weights. This new strategy allows
676 to control the order of accuracy of the interpolation close to the discontinuity but
677 not in the interval that contains it. The second strategy is inspired by the ENO-
678 SR algorithm [41]. This second algorithm manages to raise the order of accuracy
679 even at the interval that contains the discontinuity. Both strategies make use of new
680 smoothness indicators that are inspired by those presented in [36]. The new algorithms
681 have been theoretically analyzed to determine the value of the parameters t and ϵ
682 that appear in (2.10) and (3.13). It turns out that the value of these parameters is

i	Example 1			Example 2			Example 3		
	WENO	New WENO	WENO-SR	WENO	New WENO	WENO-SR	WENO	New WENO	WENO-SR
6	0.0039189	0.0050155	0.0067716	0.0037825	0.0063749	0.0055041	0.0040808	0.0060425	0.0060831
7	0.0041907	0.0064866	0.0072892	0.0032467	0.0066217	0.0074879	0.0028794	0.0070028	0.0056376
8	0.0052122	0.01333	0.0094176	0.0049805	0.0093341	0.010404	0.0046728	0.0094143	0.011844
9	0.0092705	0.021184	0.023047	0.0092013	0.019338	0.028683	0.0094946	0.018851	0.018876
10	0.01928	0.038014	0.045976	0.018954	0.034816	0.038187	0.018083	0.035791	0.036507
11	0.035951	0.061106	0.062691	0.034358	0.061173	0.060977	0.036714	0.061167	0.061914
12	0.059382	0.12116	0.12277	0.059937	0.12127	0.12286	0.059257	0.12214	0.12334

TABLE 9

In this table we present the computational time consumed by WENO, the algorithm presented in Subsection 3.2 (labeled as New WENO) and the algorithm presented in Subsection 3.3 (labeled as WENO-SR).

683 important in order to assure that the algorithms satisfy the ENO property, presented
684 in Subsection 3.4, and the accuracy requirement for which they have been designed:
685 attaining optimal accuracy control even close to kinks and jump discontinuities. The
686 numerical experiments presented confirm all the theoretical conclusions reached. This
687 work is the first one of a series of two, and is devoted to the point values version of the
688 algorithms presented. The second article [1] will be devoted to the cell averages and
689 how to implement a shock capturing scheme for the accurate solution of hyperbolic
690 conservation laws.

691 **Acknowledgments.** We would like to thank the referees and the editor for their
692 useful suggestions and comments that, with no doubt, have helped to improve the
693 quality of this paper.

694 REFERENCES

695 [1] Sergio Amat, Juan Ruiz, and Chi-Wang Shu. On new strategies to control the accuracy of
696 WENO algorithm close to discontinuities II: cell averages and conservation laws. *In preparation.*, 2018.

697 [2] Ami Harten and Stanley Osher. Uniformly high-order accurate nonoscillatory schemes. I. *SIAM*
698 *J. Numer. Anal.*, 24(2):279 – 309, 1987.

700 [3] Ami Harten, Bjorn Engquist, Stanley Osher, and Sukumar R Chakravarthy. Uniformly high
701 order accurate essentially non-oscillatory schemes, III. *J. Comput. Phys.*, 71(2):231 – 303,
702 1987.

703 [4] Chi-Wang Shu and Stanley Osher. Efficient implementation of essentially non-oscillatory shock-
704 capturing schemes. *J. Comput. Phys.*, 77(2):439 – 471, 1988.

705 [5] Chi-Wang Shu. *High Order ENO and WENO Schemes for Computational Fluid Dynamics*,
706 pages 439 – 582. Springer, Berlin, Heidelberg, 1999.

707 [6] Chi-Wang Shu and Stanley Osher. Efficient implementation of essentially non-oscillatory shock-
708 capturing schemes II. *J. Comput. Phys.*, 83(1):32 – 78, 1989.

709 [7] Francesc Arandiga, Albert Cohen, Rosa Donat, Nira Dyn, and Basarab Matei. Approximation
710 of piecewise smooth functions and images by edge-adapted (ENO-EA) nonlinear multires-
711 olution techniques. *Appl. Comput. Harmon. Anal.*, 24(2):225 – 250, 2008. Special Issue
712 on Mathematical Imaging – Part II.

713 [8] Sergio Amat, Francesc Aràndiga, Albert Cohen, Rosa Donat, Gregori Garcia, and Markus von
714 Oehsen. Data compression with ENO schemes: A case study. *Appl. Comput. Harmon.*
715 *Anal.*, 11(2):273 – 288, 2001.

716 [9] S. Serna and A. Marquina. Power ENO methods: a fifth-order accurate weighted power ENO
717 method. *J. Comput. Phys.*, 194(2):632 – 658, 2004.

718 [10] A. Cohen, N. Dyn, and B. Matei. Quasi linear subdivision schemes with applications to ENO
719 interpolation. *Appl. Comput. Harmon. Anal.*, 15:89 – 116, 2003.

720 [11] Sergio Amat, Sonia Busquier, and J. Carlos Trillo. On multiresolution schemes using a stencil
721 selection procedure: applications to ENO schemes. *Numer. Algorithms*, 44(1):45 – 68,
722 2007.

723 [12] Sergio Amat, Francesc Aràndiga, Albert Cohen, Rosa Donat, Gregori Garcia, and Markus von

724 Oehsen. Data compression with ENO schemes: A case study. *Appl. Comput. Harmon.*
 725 *Anal.*, 11(2):273 – 288, 2001.

726 [13] Xu-Dong Liu, Stanley Osher, and Tony Chan. Weighted essentially non-oscillatory schemes. *J.*
 727 *Comput. Phys.*, 115(1):200 – 212, 1994.

728 [14] G. Jiang and C.W. Shu. Efficient implementation of weighted ENO schemes. *J. Comput. Phys.*,
 729 126(1):202 – 228, 1996.

730 [15] F. Aràndiga, A. Baeza, A. M. Belda, and P. Mulet. Analysis of WENO schemes for full and
 731 global accuracy. *SIAM J. Numer. Anal.*, 49(2):893–915, 2011.

732 [16] F. Aràndiga, A.M. Belda, and P. Mulet. Point-value WENO multiresolution applications to
 733 stable image compression. *J. Sci. Comput.*, 43(2):158–182, 2010.

734 [17] Andrew K. Henrick, Tariq D. Aslam, and Joseph M. Powers. Mapped weighted essentially
 735 non-oscillatory schemes: Achieving optimal order near critical points. *J. Comput. Phys.*,
 736 207(2):542 – 567, 2005.

737 [18] Marcos Castro, Bruno Costa, and Wai Sun Don. High order weighted essentially non-oscillatory
 738 WENO-Z schemes for hyperbolic conservation laws. *J. Comput. Phys.*, 230(5):1766 – 1792,
 739 2011.

740 [19] Samala Rathna and G. Naga Raju. A modified fifth-order WENO scheme for hyperbolic
 741 conservation laws. *Comput. Math. Appl.*, 75(5):1531 – 1549, 2018.

742 [20] Cong Huang and Li Li Chen. A simple smoothness indicator for the WENO scheme with
 743 adaptive order. *J. Comput. Phys.*, 352:498 – 515, 2018.

744 [21] Jun Zhu and Jianxian Qiu. A new type of modified WENO schemes for solving hyperbolic
 745 conservation laws. *SIAM J. Sci. Comput.*, 39(3):A1089 – A1113, 2017.

746 [22] Bart S. van Lith, Jan H.M. ten Thije Boonkamp, and Wilbert L. IJzerman. Embedded WENO:
 747 A design strategy to improve existing WENO schemes. *J. Comput. Phys.*, 330:529 – 549,
 748 2017.

749 [23] Y.-T. Zhang and C.-W. Shu. Chapter 5 - ENO and WENO schemes. In Remi Abgrall and
 750 Chi-Wang Shu, editors, *Handbook of Numerical Methods for Hyperbolic Problems. Basic*
 751 *and Fundamental Issues*, volume 17 of *Handbook of Numerical Analysis*, pages xxi – xxiii.
 752 Elsevier, 2016.

753 [24] Di Sun, Feng Qu, and Chao Yan. An efficient adaptive high-order scheme based on the WENO
 754 process. *Comput. Fluids*, 140:81 – 96, 2016.

755 [25] Jun Zhu and Jianxian Qiu. A new fifth order finite difference WENO scheme for solving
 756 hyperbolic conservation laws. *J. Comput. Phys.*, 318:110 – 121, 2016.

757 [26] Xiangxiong Zhang and Chi-Wang Shu. Positivity-preserving high order finite difference WENO
 758 schemes for compressible euler equations. *J. Comput. Phys.*, 231(5):2245 – 2258, 2012.

759 [27] G. A. Gerolymos, D. Sénéchal, and I. Vallet. Very-high-order WENO schemes. *J. Comput.*
 760 *Phys.*, 228(23):8481 – 8524, December 2009.

761 [28] Yiqing Shen and Gecheng Zha. Improvement of the WENO scheme smoothness estimator. *Int.*
 762 *J. Numer. Methods Fluids*, 64(6):653–675, 2010.

763 [29] Yuanyuan Liu, Chi-Wang Shu, and Mengping Zhang. High order finite difference WENO
 764 schemes for nonlinear degenerate parabolic equations. *SIAM J. Sci. Comput.*, 33(2):939–
 765 965, 2011.

766 [30] Tong Sun. Numerical smoothness and error analysis on WENO for the nonlinear conservation
 767 laws. *Numer. Methods. Partial Differ. Equ.*, 29(6):1881–1911, 2013.

768 [31] F. Aràndiga, M. C. Martí, and P. Mulet. Weights design for maximal order WENO schemes.
 769 *J. Sci. Comput.*, 60(3):641 – 659, September 2014.

770 [32] Qin Li, Pengxin Liu, and Hanxin Zhang. Piecewise polynomial mapping method and corre-
 771 sponding WENO scheme with improved resolution. *Commun. Comput. Phys.*, 18(5):1417
 772 – 1444, 2015.

773 [33] Dinshaw S. Balsara, Sudip Garain, and Chi-Wang Shu. An efficient class of WENO schemes
 774 with adaptive order. *J. Comput. Phys.*, 326(C):780 – 804, December 2016.

775 [34] Chi-Wang Shu. *Essentially non-oscillatory and weighted essentially non-oscillatory schemes*
 776 *for hyperbolic conservation laws*, pages 325 – 432. Springer, Berlin, Heidelberg, 1998.

777 [35] Chi-Wang Shu. High order weighted essentially nonoscillatory schemes for convection domi-
 778 nated problems. *SIAM Review*, 51(1):82–126, 2009.

779 [36] Sergio Amat and Juan Ruiz. New WENO smoothness indicators computationally efficient in
 780 the presence of corner discontinuities. *J. Sci. Comput.*, 71(3):1265 – 1302, Jun 2017.

781 [37] Sergio Amat, Jacques Liandrat, Juan Ruiz, and J. Carlos Trillo. On a power WENO scheme
 782 with improved accuracy near discontinuities. *SIAM J. Sci. Comput.*, 39(6):A2472 – A2507,
 783 2017.

784 [38] Francesc Arandiga, Albert Cohen, Rosa Donat, and Nira Dyn. Interpolation and approximation
 785 of piecewise smooth functions. *SIAM J. Numer. Anal.*, 43(1):41–57, 2005.

786 [39] E. Carlini, R. Ferretti, and G. Russo. A weighted essentially nonoscillatory, large time-step
787 scheme for hamilton–jacobi equations. *SIAM J. Sci. Comput.*, 27(3):1071 – 1091, 2005.
788 [40] Guangshan Jiang and Danping Peng. Weighted ENO schemes for hamilton–jacobi equations.
789 *SIAM J. Sci. Comput.*, 21:2126–2143, 2000.
790 [41] A. Harten. ENO schemes with subcell resolution. *J. Comput. Phys.*, 83(1):148 – 184, 1989.